



The seasonal cycle of $p\text{CO}_2$ and CO_2 fluxes in the Southern Ocean: diagnosing anomalies in CMIP5 Earth system models

N. Precious Mongwe^{1,2}, Marcello Vichi^{2,3}, and Pedro M. S. Monteiro^{1,2}

¹Southern Ocean Carbon-Climate Observatory (SOCCO), CSIR, Cape Town, South Africa

²Department of Oceanography, University of Cape Town, Cape Town, South Africa

³Marine Research Institute, University of Cape Town, Cape Town, South Africa

Correspondence: Precious Mongwe (npmongwe@gmail.com)

Received: 24 August 2017 – Discussion started: 26 September 2017

Revised: 12 April 2018 – Accepted: 17 April 2018 – Published: 15 May 2018

Abstract. The Southern Ocean forms an important component of the Earth system as a major sink of CO_2 and heat. Recent studies based on the Coupled Model Intercomparison Project version 5 (CMIP5) Earth system models (ESMs) show that CMIP5 models disagree on the phasing of the seasonal cycle of the CO_2 flux ($F\text{CO}_2$) and compare poorly with available observation products for the Southern Ocean. Because the seasonal cycle is the dominant mode of CO_2 variability in the Southern Ocean, its simulation is a rigorous test for models and their long-term projections. Here we examine the competing roles of temperature and dissolved inorganic carbon (DIC) as drivers of the seasonal cycle of $p\text{CO}_2$ in the Southern Ocean to explain the mechanistic basis for the seasonal biases in CMIP5 models. We find that despite significant differences in the spatial characteristics of the mean annual fluxes, the intra-model homogeneity in the seasonal cycle of $F\text{CO}_2$ is greater than observational products. $F\text{CO}_2$ biases in CMIP5 models can be grouped into two main categories, i.e., group-SST and group-DIC. Group-SST models show an exaggeration of the seasonal rates of change of sea surface temperature (SST) in autumn and spring during the cooling and warming peaks. These higher-than-observed rates of change of SST tip the control of the seasonal cycle of $p\text{CO}_2$ and $F\text{CO}_2$ towards SST and result in a divergence between the observed and modeled seasonal cycles, particularly in the Sub-Antarctic Zone. While almost all analyzed models (9 out of 10) show these SST-driven biases, 3 out of 10 (namely NorESM1-ME, HadGEM-ES and MPI-ESM, collectively the group-DIC models) compensate for the solubility bias because of their overly exaggerated primary pro-

duction, such that biologically driven DIC changes mainly regulate the seasonal cycle of $F\text{CO}_2$.

1 Introduction

The Southern Ocean (south of 30°S) takes up about a third of the total oceanic CO_2 uptake, slowing down the accumulation of CO_2 in the atmosphere (Fung et al., 2005; Le Quéré et al., 2016; Takahashi et al., 2012). The combination of upwelling deep ocean circumpolar waters (which are rich in carbon and nutrients) and the subduction of fresh colder mid-latitude waters makes it a key region in the role of sea–air gas exchange and heat uptake (Barbero et al., 2011; Gruber et al., 2009; Sallée et al., 2013). The Southern Ocean supplies about a third of the total nutrients responsible for biological production north of 30°S (Sarmiento et al., 2004) and accounts for about 75 % of total ocean heat uptake (Frölicher et al., 2015). Recent studies suggest that the Southern Ocean CO_2 sink is expected to change as a result of anthropogenic warming; however, the sign and magnitude of the change is still disputed (Leung et al., 2015; Roy et al., 2011; Sarmiento et al., 1998; Segschneider and Bendtsen, 2013). While some studies suggest that the Southern Ocean CO_2 sink is weakening and will continue to do so (e.g., Le Quéré et al., 2007; Son et al., 2010; Thompson et al., 2011), other recent studies infer an increasing CO_2 sink (Landschützer et al., 2015; Takahashi et al., 2012; Zickfeld et al., 2008).

Although the Southern Ocean plays a crucial role as a CO_2 reservoir and regulator of nutrients and heat, it remains under-sampled, especially during the winter season (JJA)

(seasonal cycle in the Southern Hemisphere) (Bakker et al., 2014; Monteiro et al., 2010). Consequently, we largely rely on Earth system models (ESM), inversions and ocean models for both process understanding and future simulation of CO_2 processes in the Southern Ocean. The Coupled Model Inter-comparison Project (CMIP) provides an example of such a globally organized platform (Taylor et al., 2012). Although recent studies based on CMIP5 ESMs and forward and inversion models show that CMIP5 models agree on the CO_2 annual mean sink, they disagree with available observations on the phasing of the seasonal cycle of sea–air CO_2 flux ($F\text{CO}_2$) in the Southern Ocean (e.g., Anav et al., 2013; Lenton et al., 2013).

The seasonal cycle is a major mode of variability for chlorophyll (Thomalla et al., 2011) and CO_2 in the Southern Ocean (Monteiro et al., 2010; Lenton et al., 2013). The large-scale seasonal states of sea–air CO_2 fluxes ($F\text{CO}_2$) in the Southern Ocean comprise of extremes of strong summer in-gassing with a weaker in-gassing or even out-gassing in winter (Metzl et al., 2006). These extremes are linked by the autumn and spring transitions. In autumn CO_2 in-gassing weakens linked to the increasing entrainment of sub-surface waters, which are rich in dissolved inorganic carbon (DIC), (Lenton et al., 2013; Metzl et al., 2006; Sarmiento and Gruber, 2006). During spring, the increase in primary production consumes DIC at the surface and increases the ocean's capacity to take up atmospheric CO_2 (Gruber et al., 2009; Le Quére and Saltzman, 2013; Pasquer et al., 2015; Gregor et al., 2017). The increase in sea surface temperature (SST) in summer reduces surface CO_2 solubility, which counteracts the biological uptake and reduces the CO_2 flux from the atmosphere (Takahashi et al., 2002; Lenton et al., 2013).

$F\text{CO}_2$ is also spatially variable in the Southern Ocean at the seasonal scale. North of 50°S is generally the main CO_2 uptake zone (Hauck et al., 2015; Sabine et al., 2004). This region forms a major part of the Sub-Antarctic Zone and is characterized by the confluence of upwelled, colder and nutrient-rich deep circumpolar water and mid-latitude warm water (McNeil et al., 2007; Sallée et al., 2006). It is characterized by enhanced biological uptake during spring and solubility-driven CO_2 uptake due to cool surface waters (Marinov et al., 2006; Metzl, 2009; Takahashi et al., 2012). South of 60°S towards the marginal ice zone, CO_2 fluxes are largely dominated by out-gassing, driven by the upwelling of circumpolar waters, which are rich in DIC (Matear and Lenton, 2008; McNeil et al., 2007).

The inability of CMIP5 ESM to simulate a comparable $F\text{CO}_2$ seasonal cycle with available observations estimates in the Southern Ocean has been the subject of recent literature (e.g., Anav et al., 2013; Kessler and Tjiputra, 2016) and the mechanisms associated with these biases are still not well understood. This model–observation disagreement highlights that the current ESMs might not adequately capture the dominant seasonal processes driving the $F\text{CO}_2$ in the Southern Ocean. It also questions the sensitivity of models to

adequately simulate the Southern Ocean century-scale CO_2 sink and its sensitivity to climate change feedbacks (Lenton et al., 2013). Efforts to improve simulations of CO_2 properties with respect to observations in the Southern Ocean are ongoing using forced ocean models (e.g., Pasquer et al., 2015; Rodgers et al., 2014; Visinelli et al., 2016; Rosso et al., 2017). However, it remains a challenge for fully coupled simulations. In a previous study, we developed a diagnostic framework to evaluate the seasonal characteristics of the drivers of $F\text{CO}_2$ in ocean biogeochemical models (Mongwe et al., 2016). We here apply this approach to 10 CMIP5 models against observation product estimates in the Southern Ocean. The subsequent analysis is divided as follows: the methods section (Sect. 2) explains our methodological approach, followed by results (Sect. 3), which comprise four subsections. Section 3.1 explores the spatial variability of the annual mean representation of $F\text{CO}_2$ in the 10 CMIP5 models against observation product estimates; Sect. 3.2 quantifies the biases in the $F\text{CO}_2$ seasonal cycles in the 10 models. Section 3.3 investigates surface ocean drivers of $F\text{CO}_2$ changes (temperature driven solubility and primary production), and finally, Sect. 3.4 examines the source terms in the DIC surface budget (primary production, entrainment rates and vertical gradients) and their role in surface $p\text{CO}_2$ changes. The discussion (Sect. 4) is an examination of the mechanisms behind the $p\text{CO}_2$ and $F\text{CO}_2$ biases in the models. We conclude with a synthesis of the main findings and their implications.

2 Methods

The Southern Ocean is here defined as the ocean south of the Subtropical Front (STF, defined according to Orsi et al. (1995), 11.3°C isotherm at 100 m). It is divided into two main domains: the Sub-Antarctic Zone, between the STF and the Antarctic Polar Front (PF; 2°C isotherm at 200 m), and the Antarctic Zone, south of the PF. Within the Sub-Antarctic Zone and Antarctic Zone, we further partition the domain into the three main basins of the Southern Ocean, i.e., Pacific, Atlantic and the Indian zones.

2.1 Observations datasets

We used the Landschützer et al. (2014) data product ($F\text{CO}_2$ and partial pressure of CO_2 ($p\text{CO}_2$)) as the main suite of observation-based estimates against which to compare the models throughout the analysis. Landschützer et al. (2014) dataset is synthesized from Surface Ocean CO_2 Atlas version 2 (SOCAT2) observations and high-resolution winds using a self-organizing map (SOM) through a feed-forward neural network (FNN) approach (Landschützer et al., 2013). While the Landschützer et al. (2014) dataset is based on more in situ observations (SOCAT2, 15 million source measurements) (Bakker et al., 2014) in comparison to Takahashi et al. (2009) (3 million surface measurements), used

in Mongwe et al. (2016), we are nevertheless mindful that due to paucity of observations in the Southern Ocean, this data product is still subject to significant uncertainties, as discussed in Ritter et al. (2017). To evaluate the uncertainty between data products we compare the Landschützer et al. (2014) data with Gregor et al. (2017) data product – which is based on two independent empirical models: support vector regression (SVR) and random forest regression (RFR) – as well as against Takahashi et al. (2009) for $p\text{CO}_2$ in the Southern Ocean. We compare $p\text{CO}_2$ instead of $F\text{CO}_2$ firstly, because Gregor et al. (2017) only provided fugacity and $p\text{CO}_2$, and being mindful that the choice of wind product and transfer velocity constant in computing $F\text{CO}_2$ would increase the level of uncertainty (Swart et al., 2014). Secondly, while the focus of the paper is on the examination biases in the air–sea fluxes of CO_2 , the major part of our analysis is based on $p\text{CO}_2$, which primarily determines the direction and part of the magnitude of the fluxes. We find that the three data products agree on the seasonal phasing of $p\text{CO}_2$ in the Sub-Antarctic Zone, but they show differences in the magnitudes (Fig. S1). In the Antarctic Zone, all three datasets agree in both phasing and amplitude (Fig. S1). At this stage it is not clear whether this agreement is due to all the methods converging even with the sparse data or the reason for agreement is the lack of observations. Nevertheless, more independent in situ observations will be helpful to resolve this issue. In this regard float observations from the SOCCOM program (Johnson et al., 2017) and glider observations (Monteiro et al., 2015), for example, are likely to become helpful in resolving these data uncertainties in addition to ongoing ship-based measurements.

We also used the Takahashi et al. (2009) in situ $F\text{CO}_2$ dataset as a complementary source for comparison of spatial $F\text{CO}_2$ properties in the Southern Ocean. Takahashi et al. (2009) data estimates are comprised of a compilation of about 3 million surface measurements globally, obtained from 1970 to 2000 and corrected for reference year 2000. This dataset is used, as provided, on a 4° (latitude) \times 5° (longitude) resolution. Using monthly mean sea surface temperature (SST) and salinity from the World Ocean Atlas 2013 (WOA13) dataset (Locarnini et al., 2013), we reconstructed total alkalinity (TAlk) using the Lee et al. (2006) formulation. We also use this dataset as the main observations platform in Sect. 2.3. To calculate the uncertainty of the computed TAlk, we compared the calculated total alkalinity ($\text{TAlk}_{\text{calc}}$) based on ship measurements of SST and surface salinity dataset with actual observed TAlk_{obs} of the same measurements for a set of winter (August) data collected in the Southern Ocean. We found that $\text{TAlk}_{\text{calc}}$ compares well with TAlk_{obs} ($R^2 = 0.79$) (Fig. S2, Supplement). We then used this computed monthly TAlk and $p\text{CO}_2$ from Landschützer et al. (2014) to compute DIC using CO2SYS (Pierrot et al., 2006, http://cdiac.ornl.gov/ftp/co2sys/CO2SYS_calc_XLS_v2.1, last access: March 2017), using K1 and K2 from Mehrbach et al. (1973) refitted by Dickson and Millero

(1987). For interior ocean DIC, we used the Global Ocean Data Analysis Project version 2 (GLODAP2) annual means dataset (Lauvset et al., 2016). The mixed layer depth (MLD) data were taken from de Boyer Montégut et al. (2004), on a $1^\circ \times 1^\circ$ grid; the data are provided as monthly means climatology and were used as provided. We also use the satellite chlorophyll dataset from Johnson et al. (2013).

2.2 CMIP5 model data

We used 10 models from the Coupled Model Intercomparison Project version 5 (CMIP5) Earth system models (ESM) shown in Table 1. The selection criterion for the models was based on the availability of essential variables for the analysis in the CMIP5 data portal (<http://pcmdi9.llnl.gov>) at the time of writing: i.e., monthly $F\text{CO}_2$, $p\text{CO}_2$, chlorophyll, net primary production (NPP), surface oxygen, surface dissolved inorganic carbon (DIC), MLD, sea surface temperature (SST), vertical temperature fields and annual DIC for the historical scenario. The analysis is primarily based on the climatology over 1995–2005, which was selected to match a period closest to the available observational data product (Landschützer et al., 2014; 1998–2011). However, we do examine the consistency of the seasonality of $F\text{CO}_2$ over periods longer than 10 years by comparing the seasonal cycle of $F\text{CO}_2$ and temporal standard deviation of 30 years (1975–2005) vs. 10 years (1995–2005) for HadGEM2-ES and CanESM2. We find that the seasonal cycle of $F\text{CO}_2$ remains consistent ($R = 0.99$) in both HadGEM2-ES and CanESM2 over 30 years (Fig. S3). All CMIP5 model outputs were regridded into a common $1^\circ \times 1^\circ$ regular grid throughout the analysis, except for annual CO_2 mean fluxes, which were computed on the original grid for each model.

2.3 Sea–air CO_2 flux drivers: the seasonal cycle diagnostic framework

The seasonal cycle of the ocean–atmosphere $p\text{CO}_2$ gradient ($\Delta p\text{CO}_2$) is the main driver of the variability of $F\text{CO}_2$ over comparable periods (Sarmiento and Gruber, 2006; Wanninkhof et al., 2009; Mongwe et al., 2016). Wind speed plays a dual role as a driver of $F\text{CO}_2$: it drives the seasonal evolution of buoyancy-mixing dynamics, which influences the biogeochemistry and upper water column physics (but these processes are incorporated into the variability of the DIC), as well as the rate of gas exchange across the air–sea interface (Wanninkhof et al., 2013). However, because winds in the Southern Ocean do not have large seasonal variation (Young, 1999), for this analysis we neglect the role of wind as a secondary driver of the seasonal cycle of $F\text{CO}_2$. Consequently, the seasonal cycle of $F\text{CO}_2$ is directly linked to surface $p\text{CO}_2$ variability, influenced by changes in temperature, salinity, TAlk and DIC and macronutrients (Sarmiento and Gruber, 2006; Wanninkhof et al., 2009). In this analysis we use this assumption as a basis to explore how the seasonal

Table 1. A description of the 10 CMIP5 ESMs that were used in this analysis. It shows the ocean resolution, atmospheric resolution, and available nutrients for the biogeochemical component, sea-ice model, vertical levels and the marine biogeochemical component for each ESM.

Full name and source	Model name	Ocean resolution	Atmospheric resolution	Nutrients	Sea ice model	Vertical coordinate & levels	Ocean biology	Reference
Canadian Centre for Climate Modelling and Analysis, Canada	CanESM2	CanOM4 $0.9^\circ \times 1.4^\circ$	$2.8125^\circ \times 2.8125^\circ$	N (accounts for Fe limitation)	CanSIM1	z 40 levels	NPZD	Zahariev et al. (2008)
Centro Euro-Mediterraneo Sui Cambiamenti Climatici, Italy	CMCC-CESM	OPA8.2 $0.5 - 2^\circ \times 2^\circ$	$3.8^\circ \times 3.7^\circ$	P, N, Fe, Si	CICE4	z 21 levels	PELAGOS	Vichi et al. (2007)
Centre National de Recherches Météorologiques-Centre Européen de Recherche et de Formation Avancée en Calcul Scientifique, France	CNRM-CM5	NEMOv3.3 1°	1.4°	P, N, Fe, Si	GELATO5	z 42 levels	PISCES	Séférian et al. (2013)
Institut Pierre-Simon Laplace, France	IPSL-CM5A-MR	NEMO2.3 $0.5 - 2^\circ \times 2^\circ$	$2.58^\circ \times 1.25^\circ$	P, N, Fe, Si	LIM2	z 31 levels	PISCES	Séférian et al. (2013)
Max Plank Institute for Meteorology, Germany	MPI-ESM-MR	MPIOM $1.41^\circ \times 0.89^\circ$	$1.875^\circ \times 1.875^\circ$	P, N, Fe, Si	MPIOM	z 40 levels	HAMOCC5.2	Ilyina et al. (2013)
Community Earth System Model, USA	CESM1-BGC	$0.3^\circ \times 1^\circ$	$0.9^\circ \times 1.25^\circ$	(P), N, Fe, Si		z 60 levels	BEC	Moore et al. (2004)
Norwegian Earth System Model, Norway	NorESM1-ME	MICOM $0.5^\circ \times 0.9^\circ$	$2.5^\circ \times 1.9^\circ$	P, N, Fe, Si	CICE4.1	ρ 53 levels	HAMOCC	Tjiputra et al. (2013)
Geophysical Fluid Dynamics Laboratory Earth System Model, USA	GFDL-ESM2M	$0.3^\circ \times 1^\circ$	$2.5^\circ \times 2.0^\circ$	N, P, SiO ₄ , Fe	SISp2	z 50 levels	TOPAZ2	Dunne et al. (2013)
Meteorological Research Institute-Earth System Model Version 1, Japan	MRI-ESM	$0.5^\circ \times 1^\circ$		P, N	MRI.COM3	$\sigma - z$ 51 levels	NPZD	Adachi et al. (2013)
Hadley Global Environment Model 2 – Earth System, UK	HadGEM-ES	$0.3^\circ \times 1^\circ$	$2.5^\circ \times 2.0^\circ$	N, Fe, S		40 levels	Diat-HadOCC	Palmer and Totterdell (2001)

variability of temperature and DIC regulate the seasonal cycle of $p\text{CO}_2$ in CMIP5 models relative to observational product estimates.

The seasonal cycle diagnostic framework was developed as a way of scaling the relative contributions from the rates of change of SST- and the total DIC-driven changes to the seasonal cycle of $p\text{CO}_2$ on to a common DIC scale (Mongwe et al., 2016). We use the framework to explore how understanding differences emerging from the temperature- and DIC-driven CO_2 variability could be helpful as a diagnostic of the apparent observation–model seasonal cycle biases in the Southern Ocean.

The total rate of change of DIC in the surface layer consists of the contribution of air–sea exchanges, biological, vertical

and horizontal transport-driven changes (Eq. 1).

$$\left(\frac{\partial \text{DIC}}{\partial t}\right)_{\text{Tot}} = \left(\frac{\partial \text{DIC}}{\partial t}\right)_{\text{air-sea}} + \left(\frac{\partial \text{DIC}}{\partial t}\right)_{\text{Bio}} + \left(\frac{\partial \text{DIC}}{\partial t}\right)_{\text{Vert}} + \left(\frac{\partial \text{DIC}}{\partial t}\right)_{\text{Hor}} \quad (1)$$

Because we used zonal means from medium-resolution models, we assume that the horizontal terms are negligible, though we remain mindful that there could be a seasonal cycle in the divergence of the horizontal transport due to a latitudinal gradient in DIC perturbed by Ekman flow in some regions of the Sub-Antarctic Zone (Rosso et al., 2017). This leaves air–sea exchange, vertical fluxes (advection and diffusion) and biological processes as the dominant drivers of DIC.

Since temperature does not affect DIC changes directly, but only $p\text{CO}_2$ through solubility, it was necessary to scale the influence of temperature into equivalent DIC units in order to compare the influence of temperature vs. DIC control of surface $p\text{CO}_2$ variability. Thus, in order to constrain the contribution of temperature on the seasonal variability of $p\text{CO}_2$ and $f\text{CO}_2$ we derived a new synthetic temperature-linked term “DIC equivalent” (DIC_T) defined as “the magnitude of DIC change that would correspond to a change in $p\text{CO}_2$ driven by a particular temperature change”. In this way the $\Delta p\text{CO}_2$ driven solely by modeled or observed temperature change is converted into equivalent DIC units, which allows its contribution to be scaled against the observed or modeled total surface DIC change (Eq. 1). Shifts between temperature and DIC control of $p\text{CO}_2$ are in effect tipping points because they reflect major shifts in the mechanisms that drive $p\text{CO}_2$ variability. We use this as the basis to investigate the possible mechanisms behind model biases in the seasonal cycle of $p\text{CO}_2$.

This calculation of DIC_T is done in two steps: firstly, the temperature impact on $p\text{CO}_2$ is calculated using the Takahashi et al. (1993) empirical expression that linearizes the temperature dependence of the equilibrium constants.

$$\left(\frac{\partial p\text{CO}_2}{\partial t}\right)_{\text{SST}} = p\text{CO}_2 \times 0.0423 \times \left(\frac{\partial \text{SST}}{\partial t}\right) \quad (2)$$

Though this relationship between $d\text{SST}$ and $dp\text{CO}_2$ is based on a linear assumption (Takahashi et al., 1993), this formulation has been shown to hold and has been widely used in the literature (e.g., Bakker et al., 2014; Feely et al., 2004; Marinov and Gnanadesikan, 2011; Takahashi et al., 2002; Wanninkhof et al., 2009; Landschützer et al., 2018). We show in the Supplement that the extension of this expression into polar temperature ranges ($\text{SST} < 2^\circ\text{C}$) only introduces a minor additional uncertainty of 4–5 % (SM Fig. S4).

Secondly, the temperature-driven change in $p\text{CO}_2$ is converted to an equivalent DIC_T using the Revelle factor.

$$\left(\frac{\partial \text{DIC}_T}{\partial t}\right)_{\text{SST}} = \frac{\text{DIC}}{\gamma_{\text{DIC}} \times p\text{CO}_2} \left(\frac{\partial p\text{CO}_2}{\partial t}\right)_{\text{SST}} \quad (3)$$

Here we also used a fixed value for the Revelle factor ($\gamma_{\text{DIC}} = 14$), typical of polar waters in the Southern Ocean in order to assess the error linked to this assumption. We recomputed the Revelle factor in the Sub-Antarctic and Antarctic zones using annual mean climatologies of TALK, salinity, sea surface temperature and nutrients. Firstly, we examined DIC changes for the nominal range of $p\text{CO}_2$ change (340–399 μatm :1 μatm intervals) and then used this dataset to derive the Revelle factor. The range of calculated Revelle factors in the Southern Ocean was between $\gamma_{\text{DIC}} \sim 12$ and 15.5 with an average of $\gamma_{\text{DIC}} = 13.9 \pm 1.3$. This justifies our use of $\gamma_{\text{DIC}} = 14$ for the conversion of the solubility-driven $p\text{CO}_2$ change to an equivalent DIC (DIC_T) throughout the analysis. We have provided the uncertainty that this conversion makes into the

temperature constraint DIC_T by using the upper and lower limits of the Revelle factor ($\gamma_{\text{DIC}} = 12 - 15.5$) in the model framework. In the Supplement (Fig. S5) we show examples for observations in the Sub-Antarctic and Antarctic zones, which indicate that the extremes of the Revelle factor values ($\gamma_{\text{DIC}} = 12 - 15.5$) do not alter the phasing or magnitude of the relative controls of temperature or DIC on the seasonal cycle of $p\text{CO}_2$.

The rate of change of DIC was discretized on a monthly mean as follows:

$$\left(\frac{\partial \text{DIC}_T}{\partial t}\right)_{\text{SST}} \approx \left(\frac{\Delta \text{DIC}}{\Delta t}\right)_{n,l} = \frac{\text{DIC}_{n+1,l} - \text{DIC}_{n,l}}{1 \text{ month}}, \quad (4)$$

where n is time in month, l is vertical level (in this case the surface, $l = 1$). We here take the forward derivative such that November rate is the difference between 15 November and 15 December, thus being centered at the interval between the months.

Finally, to characterize periods of temperature or DIC dominance as main drivers of the instantaneous (monthly) $p\text{CO}_2$ change we subtract Eq. (1) from Eq. (4), which yields a residual indicator $M_{T\text{-DIC}}$ Eq. (5). $M_{T\text{-DIC}}$ is then used as indicator of the dominant driver of instantaneous $p\text{CO}_2$ changes in this scale monthly timescale.

$$M_{T\text{-DIC}} = \left| \left(\frac{\partial \text{DIC}_T}{\partial t}\right)_{\text{SST}} \right| - \left| \left(\frac{\partial \text{DIC}}{\partial t}\right)_{\text{Tot}} \right| \quad (5)$$

$M_{T\text{-DIC}} > 0$ indicates that the $p\text{CO}_2$ variability is dominated by the temperature-driven solubility and when $M_{T\text{-DIC}} < 0$, it indicates that $p\text{CO}_2$ changes are mainly modulated by DIC processes (i.e., biological CO_2 changes and vertical-scale physical DIC mechanisms). We also examine the following DIC processes: (i) biological DIC changes using chlorophyll, NPP, export carbon, and surface oxygen and (ii) physical DIC mechanisms using estimated entrainment rates at the base of the mixed layer. Details of this calculation are in Sect. 2.4.

In the Southern Ocean, salinity and TALK are considered lower-order drivers of the seasonal cycle of $p\text{CO}_2$ (Takahashi et al., 1993). In the Supplement (Fig. S6), we show that salinity and TALK do not play a major role as drivers of the local seasonal cycle of $p\text{CO}_2$. We do so by computing the equivalent rate of change of DIC resulting from seasonal variability of salinity and TALK as done for temperature (Eq. 2), i.e., still assuming empirical linear relationships from Takahashi et al. (1993): $\left(\frac{\ln(p\text{CO}_2)}{\ln(\text{TALK})} \approx -9.4\right)$ and $\left(\frac{\ln(p\text{CO}_2)}{\ln(\text{Sal})} = 0.94\right)$. By applying these relationships to the model data, we confirmed that salinity and TALK are indeed secondary drivers of $p\text{CO}_2$ changes, i.e., $\left[\left(\frac{\partial \text{DIC}}{\partial t}\right)_{\text{Tot}}\right]_{\text{average}} \approx 5 \mu\text{mol kg}^{-1} \text{ month}^{-1}$, while $\left[\left(\frac{\partial \text{DIC}}{\partial t}\right)_{\text{Tot}}\right]_{\text{average}} \approx 0.6 \mu\text{mol kg}^{-1} \text{ month}^{-1}$ and $\left[\left(\frac{\partial \text{DIC}}{\partial t}\right)_{\text{TALK}}\right]_{\text{maximum}} \approx 0.4 \mu\text{mol kg}^{-1} \text{ month}^{-1}$.

2.4 Entrainment mixing

CO_2 uptake by the Southern Ocean has been shown to weaken during winter linked to the entrainment of subsurface DIC as the MLD deepens (e.g., Lenton et al., 2013; Metzl et al., 2006; Takahashi et al., 2009). Here we estimate this rate of entrainment (RE) using Eq. (6), which estimates the advection of preformed DIC at the base of the mixed layer:

$$\text{RE} = U_e \left(\frac{\partial \text{DIC}}{\partial z} \right)_{\text{MLD}}, \quad (6)$$

$$\text{RE}_n = \left(\frac{\Delta \text{MLD}_n}{\Delta t} \right) \left(\frac{\Delta \text{DIC}}{\Delta z} \right)_{n, \text{MLD}}, \quad (7)$$

$$\left(\frac{\Delta \text{DIC}}{\Delta z} \right)_{n, \text{MLD}} = \frac{\text{DIC}_{n, \text{MLD}_{n+1}} - \text{DIC}_{n, \text{MLD}_n}}{\Delta z}, \quad (8)$$

in which U_e is an equivalent entrainment velocity based on the rate of change of the MLD and n is the time in months. This approximation of vertical entrainment is necessary as it is not possible to compute this term from the CMIP5 data because the vertical DIC distribution is only available as an annual means. We use the entrainment rates to estimate the influence of subsurface/bottom DIC changes on surface DIC changes and subsequently $p\text{CO}_2$ and $F\text{CO}_2$. Because we are mainly interested in the period autumn–winter, where the MLD ≥ 60 m in the Sub-Antarctic Zone and ≥ 40 m in the Antarctic Zone at this depth seasonal variations in DIC are anticipated to be minimal – these estimates can be used. The monthly and annual mean DIC from a NEMO PISCES $0.5 \times 0.5^\circ$ model output were used to estimate the uncertainty by comparing RE computed from both (Dufour et al., 2013). We found the annual and monthly estimates to be indeed comparable with minimal differences (not shown). It is noted as a caveat that this rate of entrainment is only a coarse estimate because we were using annual means and is intended only for the autumn–winter period, when MLDs are deepened.

3 Results

3.1 Annual climatological sea–air CO_2 fluxes

The annual mean climatological distribution of $F\text{CO}_2$ in the Southern Ocean obtained from observational products is spatially variable, but mainly characterized by two key features: (i) CO_2 in-gassing north of 50 – 55° S (Polar Frontal Zone, PFZ) within and north of the Sub-Antarctic Zone, and (ii) CO_2 out-gassing between the PF ($\sim 58^\circ$ S) and the marginal ice zone (MIZ, ~ 60 – 68° S) (Fig. 1a–b). Most CMIP5 models broadly capture these features; however, they also show significant differences in space and magnitude between the basins of the Southern Ocean (Fig. 1). With the exception of CMCC-CESM, which shows a northerly extended CO_2 out-gassing band between about 40 and 50° S, CMIP5 models

generally show the CO_2 out-gassing zone between 50 and 70° S, in agreement with observational estimates (Fig. 1).

The analyzed 10 CMIP5 models show a large spatial dispersion in the spatial representation of the magnitudes of $F\text{CO}_2$ with respect to observations (Fig. 1, Table 2). They generally overestimate the upwelling-driven CO_2 out-gassing (55 – 70° S) in some basins relative to observations. IPSL-CM5A, CanESM2, MPI-ESM, GFDL-ESM2M and MRI-ESM, for example, show CO_2 out-gassing fluxes reaching up to $25 \text{ g m}^{-2} \text{ yr}^{-1}$, while observations only show a maximum of $8 \text{ g m}^{-2} \text{ yr}^{-1}$ (Fig. 1). Between 40 and 56° S (Sub-Antarctic Zone), observations and CMIP5 models largely agree, showing a CO_2 in-gassing feature, which is mainly attributable to biological processes (McNeil et al., 2007; Takahashi et al., 2012). South of 65° S, in the MIZ, models generally show an excessive CO_2 in-gassing with respect to observations (with the exception of CanESM2, IPSL-CM5A-MR and CNRM-CM5). Note that as much as this bias south of the MIZ might be a true divergence of CMIP5 models from the observed ocean, it is also possibly due to the lack of observations in this region, especially during the winter season (Bakker et al., 2014; Monteiro, 2010).

Table 2 shows the pattern correlation coefficient (PCC) and the Root mean square error (RMSE), which are here used to quantify the model spatial and magnitude performances against Landschützer et al. (2014) data product. Out of the 10 models, 6 show a moderate spatial correlation with Landschützer et al. (2014) (PCC = 0.40 – 0.60), i.e., CNRM-CM5, GFDL-ESM2M, HadGEM2-ES, IPSL-CM5A-MR, CESM1-BGC, NorESME-ME and CanESM2. While MPI-ESM-MR (PCC = 0.37), MRI-ESM (PCC = 0.36) and CMCC-CESM (PCC = -0.09) show a weak to null spatial correlation with observations, the last of these is mainly due to the overestimated out-gassing region. Spatially, GFDL-ESM2M and NorESM1-ME are the most comparable to Landschützer et al. (2014), (RMSE < 9), while CCMC-CESM, CanESM2, MRI-ESM and CNRM-CM5 shows the most differences (RMSE > 15). The rest of the models show a modest comparison (RMSE 9 – 11).

NorESM1-ME and CESM1-BGC are the only 2 of the 10 models showing a consistent spatial (RMSE < 9) and magnitude (PCC ≈ 0.50) performance. From Table 2, it is evident that an appropriate representation of the spatial properties of $F\text{CO}_2$ with respect to observations does not always correspond to comparable magnitudes. CanESM2, for example, shows a good spatial comparison (PCC = 0.54), yet a poor estimation of the magnitudes (RMSE = 19.5). In this case this is caused by an overestimation of CO_2 uptake north of 55° S ($\approx -28 \text{ g m}^{-2} \text{ yr}^{-1}$) and CO_2 out-gassing ($> 25 \text{ g m}^{-2} \text{ yr}^{-1}$) in the Antarctic Zone, resulting in a net total Southern Ocean annual weak sink ($-0.05 \text{ Pg C m}^{-2} \text{ yr}^{-1}$).

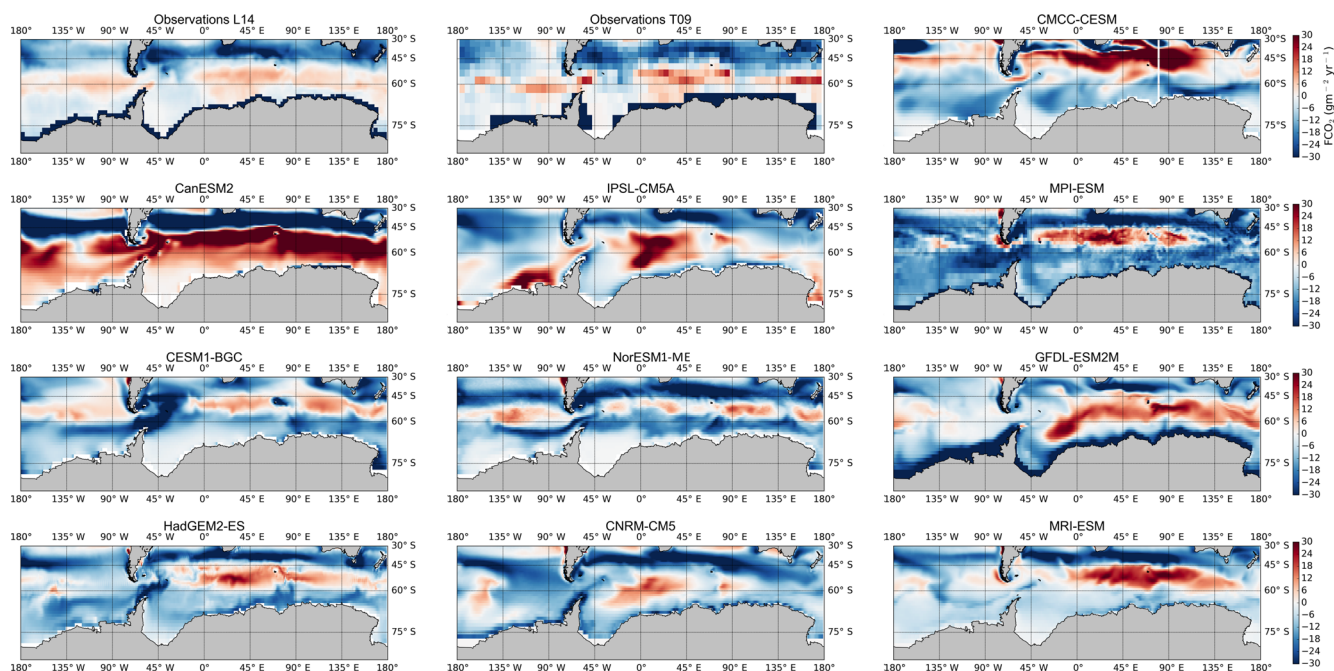


Figure 1. The annual mean climatological distribution sea–air CO_2 flux (FCO_2 , in $\text{gC m}^{-2} \text{yr}^{-1}$) for observations (L14: Landschützer et al., 2014; T09: Takahashi et al., 2009) and 10 CMIP5 models over 1995–2005. CMIP5 models broadly capture the spatial distribution of FCO_2 with respect to L14 and T09; however, they also show significant differences in space and magnitude between the basins of the Southern Ocean, with a few exceptions.

3.2 Sea–air CO_2 flux seasonal cycle variability and biases

The seasonal cycle of FCO_2 is shown in Fig. 2. The seasonality of FCO_2 in the 10 CMIP5 models shows a large dispersion in both phasing and amplitude but mostly disagrees with observations in the phase of the seasonal cycle, and the models mostly disagree among each other. More quantitatively, CMIP5 models show weak to negative correlations with the Landschützer et al. (2014) data product in the Sub-Antarctic Zone and have slightly higher correlations in the Antarctic Zone (see Supplement Fig. S7). This discrepancy is consistent with the findings of Anav et al. (2013), who, however, used fixed latitude criteria. Based on the phasing, the seasonality of FCO_2 in CMIP5 models can be a priori divided into two main groups: (1) group-DIC models, comprising MPI-ESM, HadGEM-ES and NorESM1-ME, and group-SST models, and (2) the remainder, i.e., GFDL-ESM2M, CMCC-CESM, CNRM-CERFACS, IPSL-CM5A-MR, CESM1-BGC, MRI-ESM and CanESM2. The naming convention is suggestive of the mechanism driving the seasonal cycle, as will be clarified further on. A similar grouping was also identified by Kessler and Tjiputra (2016) using a different criterion. Figure 3 shows the seasonal cycle of FCO_2 of an equally weighted ensemble of the two groups compared to observations; the shaded area shows the decadal standard deviation for the models and the Landschützer et

al. (2014) data product for 1998–2014 standard deviation in the various regions.

In the Sub-Antarctic Zone, the observational products show a weakening of CO_2 uptake during winter (less negative values in June–August) with values close to the zero at the onset of spring (September) in all three basins. Similarly, during the spring season, all three basins are seen to maintain a steady increase in CO_2 uptake until mid-summer (December), while they differ during autumn (March–May). The Pacific Basin shows an increase in CO_2 uptake during autumn that is not observed in the other basins (only marginally in the Indian zone). In the Antarctic Zone, the observed FCO_2 seasonal cycle is mostly similar in all three basins (Fig. 3d–f). While this seasonal cycle consistency may suggest a spatial uniformity of the mechanisms of FCO_2 at the Antarctic, we are also mindful that this may be due to a result of the paucity of observations in this area. In the Antarctic Zone, all three basins show a weakening of uptake or increasing of out-gassing from the onset of autumn (March) until mid-winter (June–July). The winter CO_2 out-gassing is followed by a strengthening of the CO_2 uptake throughout spring to summer, when it reaches a CO_2 in-gassing peak.

The differences in the seasonal cycle of FCO_2 across the three basins of the Sub-Antarctic Zone found in the observational product (Fig. 2) are likely a consequence of spatial differences seen in Fig. 1. To verify this, we calculated the correlation between the seasonal cycles from the Landschützer

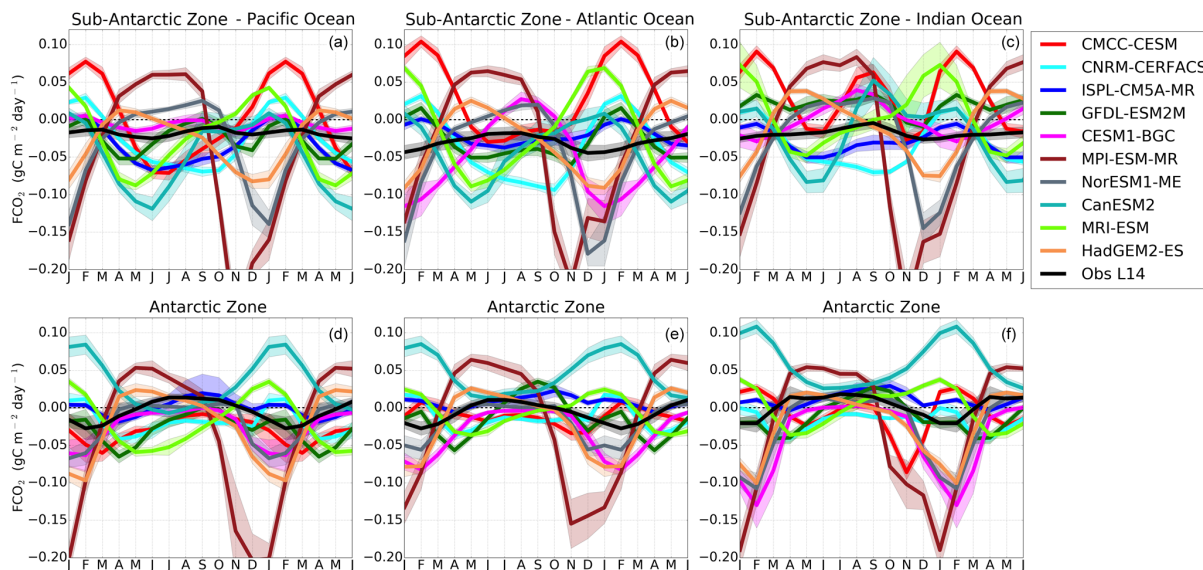


Figure 2. Seasonal cycle of sea–air CO_2 flux (FCO_2 , in $\text{gC m}^{-2} \text{ yr}^{-1}$) in observations and 10 CMIP5 models in the Sub-Antarctic and Antarctic zones of the Pacific Ocean (first column), Atlantic Ocean (second column) and Indian Ocean (third column). The shaded area shows the temporal standard deviation over the considered period (1995–2005).

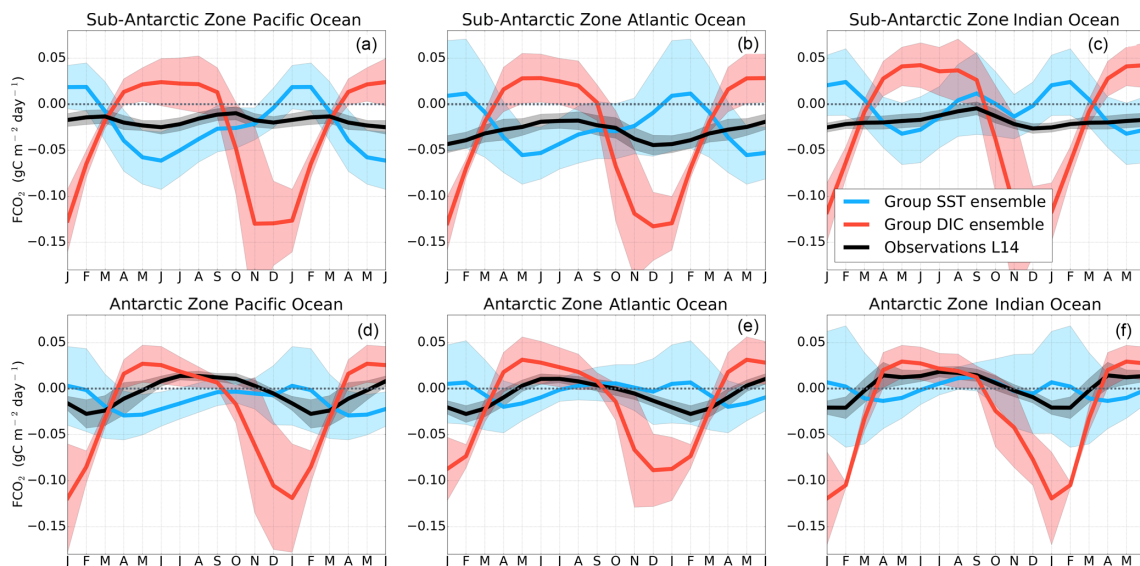


Figure 3. Seasonal cycle of the equally weighted ensemble means of FCO_2 ($\text{gC m}^{-2} \text{ yr}^{-1}$) from Fig. 2 for group DIC models (MPI-ESM, HadGEM-ES and NorESM) and group SST models (GFDL-ESM2M, CMCC-CESM, CNRM-CERFACS, IPSL-CM5A-MR, CESM1-BGC, NorESM2, MRI-ESM and CanESM2). The shaded areas show the ensemble standard deviation. The black line is the Landschützer et al. (2014) observations.

et al. (2014) observational product in the three basins (Fig. 4). The FCO_2 seasonal cycle in the Sub-Antarctic Atlantic and Indian basins are similar ($R = 0.8$), while the other basins are quite different to one another ($R = -0.1$ for Pacific–Atlantic and $R \sim 0.4$ for Pacific–Indian). Contrary to the observational product, CMIP5 models show the same seasonal cycle phasing across all three basins in the Sub-Antarctic Zone (basin–basin correlation coefficients are always larger than

0.50 in Fig. 4 despite the spatial differences in Fig. 2, with the exception of three models, i.e., CMCC-CESM, CESM-BGC1 and GFDL-ESM2M). Thus, contrary to Landschützer et al. (2014), CMIP5 models show a zonal homogeneity in the seasonal cycle of FCO_2 , which may suggest that the drivers of CO_2 are less regional. In the Antarctic Zone, CMIP5 models agree with observations in the spatial uniformity of the seasonal cycle of FCO_2 across the three basins.

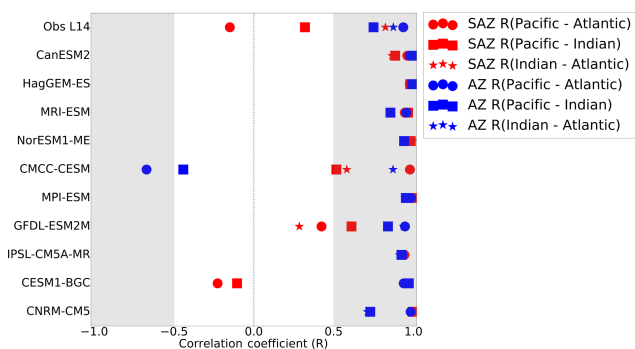


Figure 4. The correlation coefficients (R) of basin–basin seasonal cycles of $F\text{CO}_2$ for observations (Landschützer et al., 2014) and 10 CMIP5 models in the three basins of the Southern Ocean, i.e., Pacific, Atlantic and Indian basins.

Group-DIC models are characterized by an exaggerated CO_2 uptake during spring–summer (Fig. 3) with respect to observation estimates and CO_2 out-gassing during winter. These models generally agree with observations in the phasing of CO_2 uptake during spring, but overestimate the magnitudes. It is worth noting that the seasonal characteristics of group-DIC models are mostly in agreement with the observations in the Atlantic and Indian basins in Sub-Antarctic Zone ($R > 0.5$ in Fig. 4). The large standard deviation ($\sim 0.01 \text{ g C m}^{-2} \text{ day}^{-1}$) during the winter and spring–summer seasons in the Atlantic Basin shows that though group-DIC models agree in the phase, magnitudes vary considerably (Fig. 3b). For example MPI-ESM reaches up to $0.06 \text{ g C m}^{-2} \text{ day}^{-1}$ out-gassing during winter, while HadESM2-ES and NorESM2 peak only at $\sim 0.03 \text{ g C m}^{-2} \text{ day}^{-1}$. Group-SST models on the other hand are characterized by a CO_2 out-gassing peak in summer (December–February) and a CO_2 in-gassing peak at the end of autumn (May), and their phase is opposite to the observational estimates in the Atlantic and Indian basins (Fig. 3b, c). Group-SST models only show a strengthening of CO_2 uptake during spring in the Indian Basin. Interestingly, group-SST models compare relatively well with the observed $F\text{CO}_2$ seasonal cycle in the Pacific Basin, whereas group-DIC models disagree the most with the observed estimates (Fig. 3a). This phasing difference within models and against observed estimates probably suggests that the disagreement of CMIP5 models $F\text{CO}_2$ with observations is not a matter of a relative error/constant magnitude offset but most likely points to differences in the seasonal drivers of $F\text{CO}_2$.

In the Antarctic Zone (Fig. 3d–f), both group-DIC and group-SST models perform better than in the Sub-Antarctic, with respect to phasing and amplitude in as shown by the correlation analysis in Fig. S7. Models reflect comparable $p\text{CO}_2$ seasonality in the different basins of the AZ to the observational products (Fig. 4, with the exception of MRI-ESM and CanESM2, where $R < 0$ for

all three basins). Here $F\text{CO}_2$ magnitudes oscillate around zero with the largest disagreements occurring during mid-summer, where observation estimates show a weak CO_2 sink ($\approx -0.03 \text{ g C m}^{-2} \text{ day}^{-1}$), and group-SST show a zero net CO_2 flux and a strong uptake in group DIC (e.g., $\approx -0.12 \text{ g C m}^{-2} \text{ day}^{-1}$ in the Pacific Basin). The large standard deviation ($\approx 0.01 \text{ g C m}^{-2} \text{ day}^{-1}$) here indicates considerable differences among models (Fig. 3d–f).

3.3 Seasonal-scale drivers of sea–air CO_2 flux

We now examine how changes in temperature and DIC regulate $F\text{CO}_2$ variability at the seasonal scale following the method described in Sect. 2.3. Figure 5 shows the monthly rates of change of SST ($d\text{SST}/dt$) for the 10 models compared with WOA13 SST. CMIP5 generally shows agreement in the timing of the switch from surface cooling ($d\text{SST}/dt < 0$) to warming ($d\text{SST}/dt > 0$) and vice versa, i.e., March (summer to autumn) and September (winter to spring), respectively. In both the Sub-Antarctic and Antarctic Zone CMIP5 models agree with observations in this timing (Fig. 5). However, while they agree in phasing, the amplitude of these warming and cooling rates are overestimated with respect to the WOA13 dataset with the exception of NorESM1-ME. Subsequently these differences in the magnitude of $d\text{SST}/dt$ have important implications for the solubility of CO_2 in seawater, with larger magnitudes of $|d\text{SST}/dt|$ likely to enhance the response of the $p\text{CO}_2$ to temperature through CO_2 solubility changes. For example, because the observations in the Indian Basin show a warming rate of about $0.5 \text{ }^\circ\text{C month}^{-1}$ lower compared to the other two basins, we expect a relatively weaker role of surface temperature in this basin.

As described in Sect. 2.3, the computed $d\text{SST}/dt$ magnitudes were used to estimate the equivalent rate of change of DIC driven by CO_2 solubility using Eq. (2). The seasonal cycle of $|(d\text{DIC}_T/dt)_{\text{SST}}|$ vs. $|(d\text{DIC}/dt)_{\text{Tot}}|$, for the 10 models and observations is presented in the Supplement (Fig. S8), where we show the seasonal mean of $M_{T\text{-DIC}}$ from (Eq. 3). As articulated in Sect. 2.3, $M_{T\text{-DIC}}$ (Fig. 6) is the difference between the total surface DIC rate of change of DIC (Eq. 1) and the estimated equivalent temperature-driven solubility DIC changes Eq. (3), such that when $|(d\text{DIC}_T/dt)_{\text{SST}}| > |(d\text{DIC}/dt)_{\text{Tot}}|$, temperature is the dominant driver of the instantaneous $p\text{CO}_2$ changes, and conversely when $|(d\text{DIC}_T/dt)_{\text{SST}}| < |(d\text{DIC}/dt)_{\text{Tot}}|$, DIC processes are the dominant mode in the instantaneous $p\text{CO}_2$ variability. The models showing the former feature are SST-driven and belong to group-SST, while the models showing the latter are DIC-driven and belong to group-SST.

According to the $M_{T\text{-DIC}}$ magnitudes in Fig. 6, the seasonal cycle of $p\text{CO}_2$ in the observational estimates is predominantly DIC-driven most of the year in both the Sub-Antarctic and Antarctic Zone. Note that, however, during periods of high $|d\text{SST}/dt|$, i.e., autumn and spring, observa-

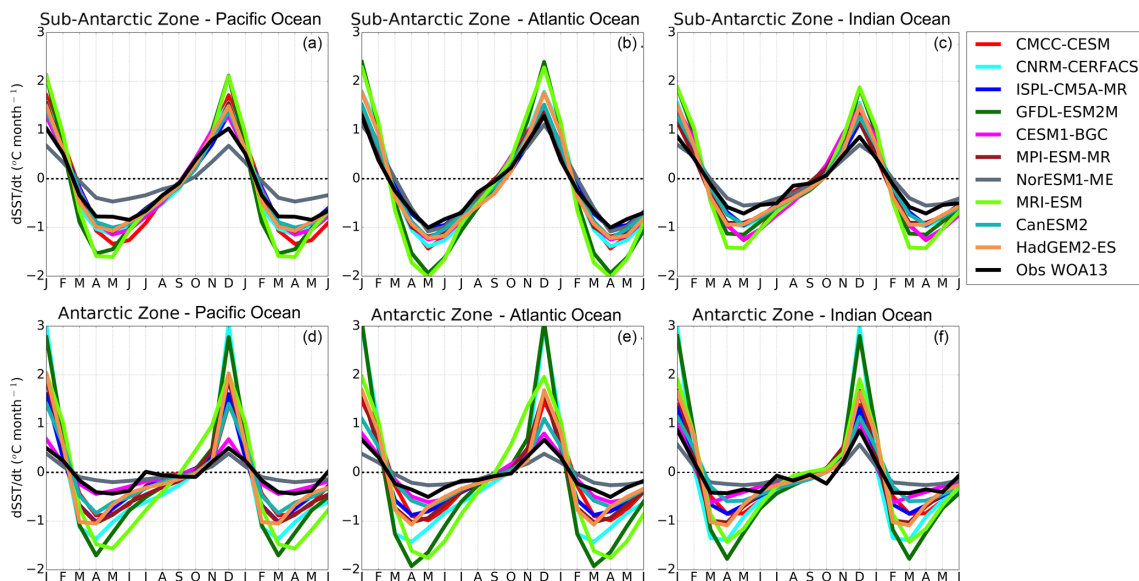


Figure 5. Mean seasonal cycle of the estimated rate of change of sea-surface temperature ($d\text{SST}/dt$, $^{\circ}\text{C month}^{-1}$) for the Sub-Antarctic and Antarctic zones of the Pacific Ocean (first column), Atlantic Ocean (second column) and Indian Ocean (third column).

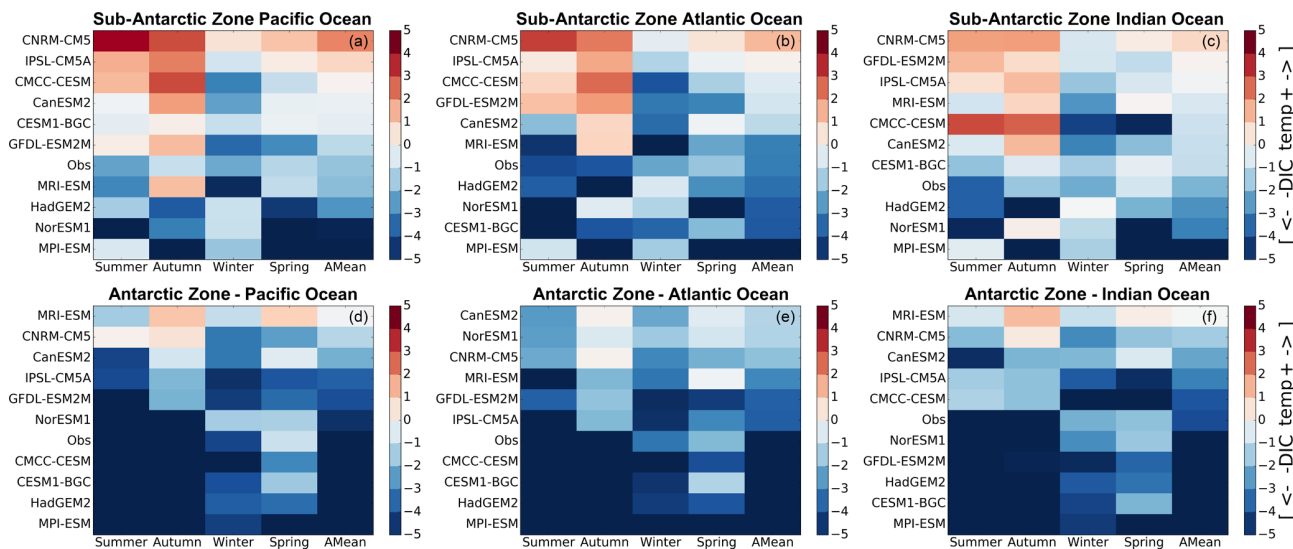


Figure 6. Mean seasonal and annual values of the DIC–temperature control index ($M_{T\text{-DIC}}$). The increase in the red color intensity indicates increase in the strength of the temperature driver and the blue intensity shows the strength of the DIC driver. The models are sorted according to the annual mean value of the indicator presented in the last column (AMean).

tions show a moderate to weak DIC control ($M_{T\text{-DIC}} \approx 0$). The Antarctic Zone is mostly characterized by a stronger DIC control (mean annual $M_{T\text{-DIC}} > 0$) except for during the spring season (Fig. 6). Consistent with the similarity analysis presented in Fig. 4, the Antarctic Zone shows coherence in the sign of the temperature–DIC indicator ($M_{T\text{-DIC}} > 0$) within the three basins.

3.4 Source terms in the DIC surface budget

To further constrain the surface DIC budget in Eq. (1), we examine the role of the biological source term using chlorophyll and net primary production (NPP) as proxies. Figure 8 shows the seasonal cycle of chlorophyll, NPP and the rate of surface DIC changes ($d\text{DIC}/dt$). The observed seasonal cycle of chlorophyll (Johnson et al., 2013) shows a similar seasonal cycle within the three basins during the spring–summer seasons (autumn–winter data are removed due to the

satellite limitation) in both the Sub-Antarctic and Antarctic Zone. Magnitudes are, however, different in the Sub-Antarctic Zone; the Atlantic Basin shows larger chlorophyll magnitudes (chlorophyll reach up to 1.0 mg m^{-3}) compared to the Pacific and Indian basins ($\text{Chl} < 1 \text{ mg m}^{-3}$).

CMIP5 models here show a clear partition between group-DIC and group-SST models. While they mostly maintain the same phase, group-DIC shows larger amplitudes of chlorophyll relative to group-SST and observed estimates in the Sub-Antarctic Zone. This difference is even clearer in NPP magnitudes, where group-DIC models show a maximum of $\text{NPP} > 1 \text{ mmol m}^{-2} \text{ s}^{-1}$ in summer, while group-SST magnitudes shows about half of it. Except for CESM1-BGC and CMCC-CESM (and NorESM1-ME for NPP), each CMIP5 model generally maintains a similar chlorophyll seasonal cycle (phase and magnitude) in all three basins of the Southern Ocean. This is contrary to the observations, which show differences in the magnitude. Consistent with the observational product, CESM1-BGC simulates larger amplitude in the Atlantic Basin. While CMCC-CESM also has this feature, it also shows an overestimated chlorophyll peak in the Indian Basin. In the Antarctic Zone both observations and CMIP5 models generally agree in both phase and magnitude (except for CanESM2) of the seasonal cycle of chlorophyll in all three basins.

We now examine the influence of the vertical DIC rate in Eq. (1), using estimated entrainment rates (RE, Eq. 5) based on MLD and vertical DIC gradients (see Sect. 2.3). Figure 7 shows the seasonal changes of MLD compared with the rate from the observational product. CMIP5 models largely agree on the timing of the onset of MLD deepening (February in the Pacific Basin, and March for the Atlantic and Indian basins) and shoaling (September) in the Sub-Antarctic Zone (with the exception of NorESM1-ME and IPSL-CM5A in the Pacific Basin). The Indian Basin generally shows deeper winter MLD in both observations and CMIP5 models in the Sub-Antarctic Zone. Note that while CMIP5 models generally show the observed deeper MLDs in the Indian Basin, they show a large variation; for example, the winter maximum depth ranges from 100 m (CMCC-CESM, Pacific Basin) to 350 m (CanESM2, Indian Basin) in the Sub-Antarctic Zone. In the Antarctic Zone CMIP5 models are largely in agreement on the timing of the onset of MLD deepening (February) but also variable in their winter maximum depth. It is worth noting that the observed MLD seasonal cycle might be biased due to limited in situ observations particularly in the Antarctic Zone (de Boyer Montégut et al., 2004).

The estimated RE values in Fig. 10 show that almost all CMIP5 models (with the exception of NorESM1-ME) entrain subsurface DIC into the mixed layer during autumn–winter, in agreement with the observational estimates. In the Sub-Antarctic Zone, the estimates using the observational products show the strongest entrainment in the Atlantic Basin in May (RE reaches up to $10 \mu\text{mol kg}^{-1} \text{ month}^{-1}$), while it is lower in the other basins. In the Antarctic Zone, observed RE

conversely shows stronger entrainment rates in the Pacific and Indian basins ($\text{RE} > 15 \mu\text{mol kg}^{-1} \text{ month}^{-1}$) in comparison to the Atlantic Basin ($\text{RE} = 11 \mu\text{mol kg}^{-1} \text{ month}^{-1}$). CMIP5 models entrainment rates are variable but not showing any particular deficiency when compared with the observational estimates. Also, the group-DIC and group-SST models show no clear distinction, the major striking features being the relatively stronger entrainment in MPI-ESM and CanESM2 across the three basins in the Sub-Antarctic Zone in mid- to late winter ($\text{RE} = 15 \mu\text{mol kg}^{-1} \text{ month}^{-1}$), and the large winter entrainment in IPSL-CM5A-MR in the Antarctic Pacific Basin. The supply of DIC to the surface due to vertical entrainment is therefore generally comparable between model simulations and the available estimate.

However, our RE estimates are estimated at the base of the mixed layer, which is not necessarily a complete measure of the vertical flux of DIC at the surface. We therefore investigate the annual mean vertical DIC gradients in Fig. 10 as an indicator of where the surface uptake processes occur. The simulated CMIP5 profiles are similar to GLODAP2, but some differences arise. In the Sub-Antarctic Zone, GLODAP2 shows a shallower surface maximum in the Atlantic Basin consistent with higher biomass in this basin (Fig. 8) ($(\text{dDIC}/\text{dz})_{\text{max}} = 0.55 \mu\text{mol kg}^{-1} \text{ m}^{-1}$, at 50 m) compared to the Pacific ($(\text{dDIC}/\text{dz})_{\text{max}} = 0.60 \mu\text{mol kg}^{-1} \text{ m}^{-1}$, at 80 m) and Indian Basin ($(\text{dDIC}/\text{dz})_{\text{max}} = 0.40 \mu\text{mol kg}^{-1} \text{ m}^{-1}$, at 80 m). CMIP5 models generally do not show this feature in the Sub-Antarctic Zone, except for CESM1-BGC1 ($(\text{dDIC}/\text{dz})_{\text{max}} = 0.50 \mu\text{mol kg}^{-1} \text{ m}^{-1}$, at 50 m). Instead, they show the surface maxima at the same depth in all three basins. In the Antarctic Zone both CMIP5 models and observations show larger $(\text{dDIC}/\text{dz})_{\text{max}}$ magnitudes and nearer surface maxima (with the exception of CanESM2 and CESM1-BGC). This difference in the position and magnitude of the DIC maxima between the Sub-Antarctic and Antarctic Zone has important implications for surface DIC changes and subsequently $p\text{CO}_2$ seasonal variability. Because of the nearer surface DIC maxima in the Antarctic Zone, surface DIC changes are mostly influenced by these strong near-surface vertical gradients compared to MLD changes. This implies that even if the entrainment rates at the base of the MLD are comparable between the Sub-Antarctic and the Antarctic, the surface supply of DIC may be larger in the Antarctic Zone.

4 Discussion

Recent studies have highlighted that important differences exist between the seasonal cycle of $p\text{CO}_2$ in models and observations in the Southern Ocean (Lenton et al., 2013; Anav et al., 2015; Mongwe, 2016). Paradoxically, although the models may be in relative agreement for the mean annual flux, they diverge in the phasing and magnitude of the sea-

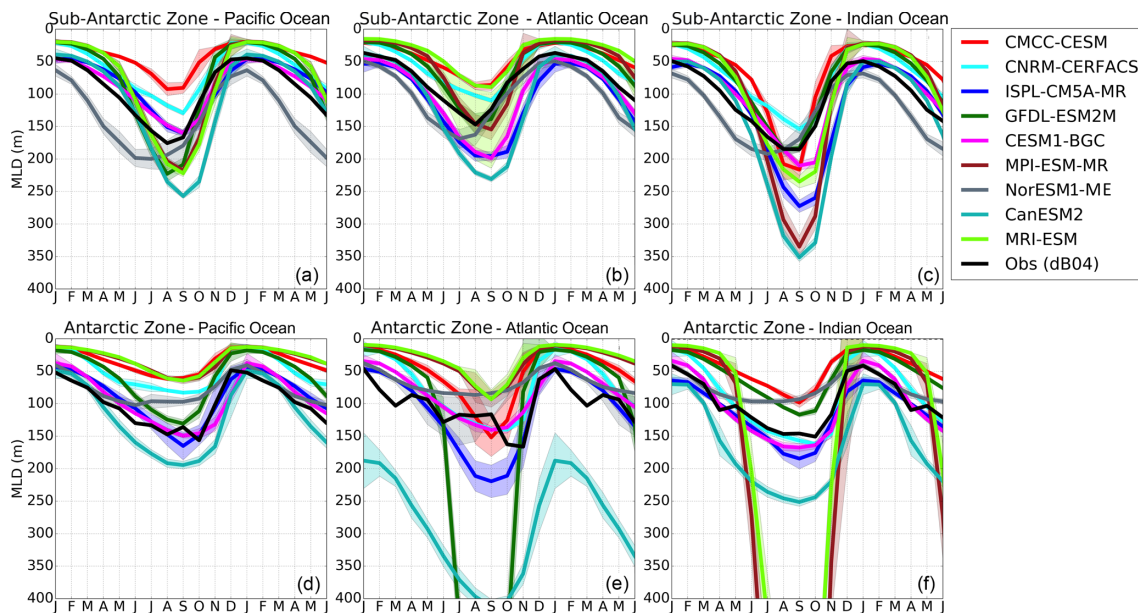


Figure 7. Seasonal cycle of the mixed layer depth (MLD) in the Sub-Antarctic and Antarctic zones of the Pacific Ocean (first column), Atlantic Ocean (second column) and Indian Ocean (third column).

sonal cycle (Lenton et al., 2013; Anav et al., 2015; Mongwe, 2016). These differences in the seasonal cycle raise questions about the climate sensitivity of the carbon cycle in these models because they may reflect differences in the process sensitivities to drivers that are themselves climate sensitive.

In this study we expand on the framework proposed by Mongwe et al. (2016), which examined the competing roles of temperature and DIC as drivers of $p\text{CO}_2$ variability and the seasonal cycle of $p\text{CO}_2$ in the Southern Ocean, to explain the mechanistic basis for seasonal biases of $p\text{CO}_2$ and $F\text{CO}_2$ between observational products and CMIP5 models. This analysis of 10 CMIP5 models and one observational product (Landschützer et al., 2014) highlighted that although the models showed different seasonal cycles (Fig. 2), they could be grouped into two categories (SST- and DIC-driven) according to their mean seasonal bias of temperature or DIC control (Figs. 3, 6).

A few general insights emerge from this analysis. Firstly, despite significant differences in the spatial characteristics of the mean annual fluxes (Fig. 1), models show unexpectedly greater inter-basin coherence in the phasing seasonal cycle of $F\text{CO}_2$ and SST-DIC control than observational products (Fig. 3, 6). Clear inter-basin differences have been highlighted in studies on the climatology and interannual variability that examined $p\text{CO}_2$ and CO_2 fluxes based on data products (Landschützer et al., 2015; Gregor et al., 2017), as well as phytoplankton chlorophyll based on remote sensing (Thomalla et al., 2011; Carranza et al., 2016). Briefly, the Atlantic Basin shows the highest mean primary production in contrast to the Pacific Basin, which has the lowest (Thomalla et al., 2011). Similarly, strong inter-basin differences for

$p\text{CO}_2$ and $F\text{CO}_2$ have been highlighted and ascribed to SST control (Landschützer et al., 2016) and wind stress–mixed layer depth (Gregor et al., 2017). The combined effect of these regional differences in forcing of $p\text{CO}_2$ and $F\text{CO}_2$ would be expected to be reflected in the CMIP5 models as well. A quantitative analysis of the correlation of the phasing of the seasonal cycle of $F\text{CO}_2$ between basins for different models shows that all the models except three (CMCC-CESM, GFDL-ESM2M, CESM1-CESM) are characterized by strong inter-basin correlation in both the Sub-Antarctic and Antarctic zones (Fig. 4). This suggests that the carbon cycle in these CMIP5 models is not sensitive to inter-basin differences in the drivers as is the case for observations. This most likely implies that CMIP5 models are not sensitive to regional $F\text{CO}_2$ variability at the basin scale, so $F\text{CO}_2$ seasonal biases are zonally uniform.

Secondly, an important part of this analysis is based on the assumption that the observational products that are used to constrain the spatial and temporal variability of $p\text{CO}_2$ and $F\text{CO}_2$ reflect the correct seasonal cycles of the Southern Ocean. This assumption requires significant caution not only due to the limitations in the sparseness of the in situ observations but also due to limitations of the empirical techniques in overcoming these data gaps (Landschützer et al., 2014; Rödenbeck et al., 2015; Gregor et al., 2017, 2018; Ritter et al., 2017). The uncertainty analysis from these studies suggests that, while the seasonal bias in observations may be less in the Sub-Antarctic Zone and PFZ, it is the highest in the AZ, where access is limited mostly to summer and winter ice cover results in uncertainties that may limit the significance of the data–model comparisons. It is impor-

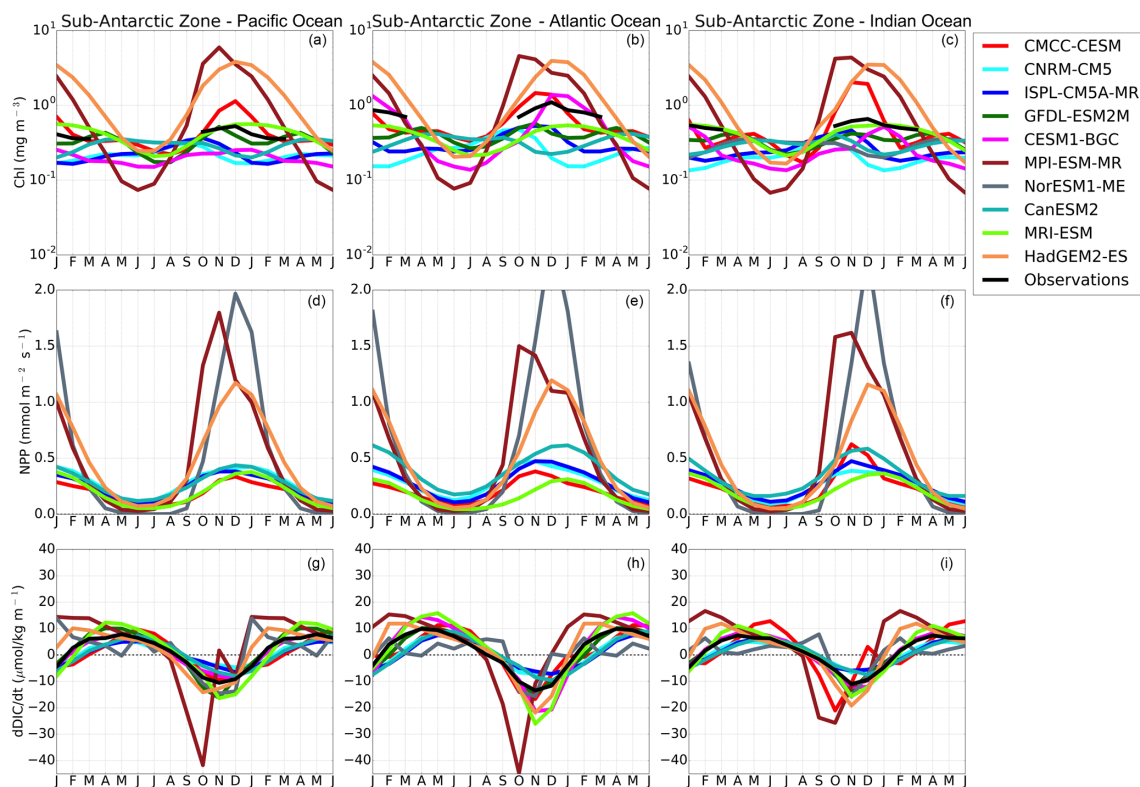


Figure 8. The seasonal cycle of chlorophyll (mg m^{-3}), net primary production ($\text{mmol m}^{-2} \text{s}^{-1}$) and the surface rate of change of DIC ($\mu\text{mol kg}^{-1} \text{month}^{-1}$) in the Sub-Antarctic Zone of the Pacific Ocean (first column), Atlantic Ocean (second column) and Indian Ocean (third column).

tant to note that though the observation product that we use here (Landschützer et al. (2014) is based on more surface measurement (10 million, SOCAT v3) compared to previous datasets (e.g., Tahakahashi et al., 2009, 3 million), the data are still sparse in time and space in the Southern Ocean. Thus, in using this data product as our main observational estimates for this analysis we are mindful of the limitations in the discussion below.

Thirdly, the seasonal cycle of $\Delta p\text{CO}_2$ is the dominant mode of variability in $F\text{CO}_2$ (Mongwe et al., 2016; Wanninkhof et al., 2009). Though winds provide the kinematic forcing for air–sea fluxes of CO_2 and indirectly affect $F\text{CO}_2$ through mixed layer dynamics and associated biogeochemical responses (Mahadevan et al., 2012; du Plessis et al., 2017), $\Delta p\text{CO}_2$ sets the direction of the flux. Surface $p\text{CO}_2$ changes are mainly driven by DIC and SST (Hauck et al., 2015; Takahashi et al., 1993). Subsequently the sensitivity of CMIP5 models to how changes in DIC and SST regulate the seasonal cycle of $F\text{CO}_2$ is fundamental to the model’s ability to resolve the observed $F\text{CO}_2$ seasonal cycle. Thus, here we examined the influence of DIC and SST on $F\text{CO}_2$ at seasonal scale for 10 CMIP5 models with respect to observed estimates. Because temperature does not directly affect DIC changes, we first scaled up the impact of SST changes on $p\text{CO}_2$ through surface CO_2 solubility to equivalent DIC units

using the Revelle factor (Sect. 2.3). In this way, we can distinguish the influence of surface solubility and DIC changes (i.e., biological and physical) on $p\text{CO}_2$ and hence on $F\text{CO}_2$.

Fourthly, using this analysis framework (Sect. 2.3, summarized in Fig. 6) we found that CMIP5 models $F\text{CO}_2$ biases cluster in two groups, namely group-DIC ($M_{T\text{-DIC}} < 0$) and group-SST ($M_{T\text{-DIC}} > 0$). Group-DIC models are characterized by an overestimation of the influence of DIC on $p\text{CO}_2$ with respect to observations estimates, which instead indicate that physical and biogeochemical changes in the DIC concentration mostly regulate the seasonal cycle of $F\text{CO}_2$ (in short, DIC control). Group-SST models show an excessive temperature influence on $p\text{CO}_2$; here surface CO_2 solubility biases are mainly responsible for the departure of modeled $F\text{CO}_2$ from the observational products. While CMIP5 models mostly show a singular dominant influence of these extremes, observations show a modest influence of both, with a dominance of DIC changes as the main driver of seasonal $F\text{CO}_2$ variability. Below we discuss the seasonal cycle characteristics and possible mechanisms for these two groups of CMIP5 models in the Sub-Antarctic and Antarctic zones of the Southern Ocean.

4.1 Sub-Antarctic Zone (SAZ)

Our diagnostic analysis indicates that the seasonal cycle of $p\text{CO}_2$ in the observational product (Landschützer et al., 2014) is mostly DIC controlled across all three basins of the SAZ ($M_{T\text{-DIC}} < 0$ in Fig. 6). The Atlantic Basin shows a stronger DIC control (annual mean $M_{T\text{-DIC}} \geq 2$) compared to the Pacific and Indian basins (annual mean $M_{T\text{-DIC}} \approx 1$). This stronger influence of DIC on $p\text{CO}_2$ in the Atlantic Basin is consistent with higher primary production in this basin (Graham et al., 2015; Thomalla et al., 2011), here shown by the larger mean seasonal chlorophyll from remote sensing in the Atlantic Basin with respect to the Pacific and Indian basins (Fig. 8). This significant basin difference is most likely linked to the fact that the Atlantic Basin has longer periods of shallow MLD compared to the Pacific and Indian basins (Fig. 7a–c, November–March and November–February, respectively) and has been shown to have higher supplies of continental shelves and land-based iron (Boyd and Ellwood, 2010; Tagliabue et al., 2012, 2014). These conditions are more likely to enhance primary production that translates into a higher rate of change of surface DIC (Fig. 8), which becomes the major driver of $F\text{CO}_2$ variability. In contrast, shorter periods of shallow MLD and lower iron inputs in the Pacific Basin (Tagliabue et al., 2012) likely account for a lower chlorophyll biomass and hence the weaker DIC control evidenced in our analysis ($M_{T\text{-DIC}} \approx 0$ in Fig. 6). In the Indian Basin, the winter mixed layer is deeper than in the Atlantic and deepens earlier in the season (Fig. 7c). These conditions limit chlorophyll concentration (Fig. 8) and possibly contribute to the lower rates of surface temperature change because of the enhanced mixing (cf. Fig. 5a–c). As a consequence, the resulting net driver in the Indian and Pacific basins is a weaker DIC control, because both biological DIC and solubility changes are relatively weaker and they oppose each other. Because of this, when the magnitudes of the rate of change of SST are larger during cooling and warming seasonal peaks (autumn and spring, respectively), DIC control is weaker ($M_{T\text{-DIC}} \approx 0$) during these seasons.

CMIP5 models do not capture these basin-specific features as demonstrated with the correlation analysis in Fig. 4, with the exception of three group-SST models (i.e., CESM1-BGC, GFDL-ESM2M and CMCC-CESM). These, in contrast, mostly show comparable $F\text{CO}_2$ phasing in the three basins. The seasonal cycle of CO_2 flux in the Southern Ocean (Fig. 4) is both zonally and meridionally uniform for most CMIP5 models, in contrast to observational data product (Fig. 3). This suggests that CMIP5 models show equal sensitivity to basin-scale $F\text{CO}_2$ drivers, suggesting that $p\text{CO}_2$ and $F\text{CO}_2$ driving mechanisms are less local than for observations. Thus the understanding of fine-scale (mesoscale and sub-mesoscale) processes responsible for basin-scale $F\text{CO}_2$ variability will be an important contribution to the next generation of ESM. Studies based on new available data from higher-resolution autonomous platforms like Monteiro

et al. (2015), Williams et al. (2017), Briggs et al. (2018) and Rosso et al. (2017) may be useful constraints to these dynamics in ESMs.

The major feature of group-SST models in the SAZ is the out-gassing during summer and in-gassing mid-autumn to winter (Fig. 3a–c, April–August), which our diagnostics in Fig. 6 attribute to temperature (solubility) control. The summer period coincides with the highest warming rates ($d\text{SST}/dt$, Fig. 5a–c), and associated reduction in solubility of CO_2 . Similarly, exaggerated cooling rates at the onset of autumn (Fig. 5a–c) enhance CO_2 solubility, causing a change in the direction of $F\text{CO}_2$ into strengthening CO_2 in-gassing (Fig. 3a–c). Thus, while group-SST models have a seasonal amplitude of $F\text{CO}_2$ comparable to observations, they are out of phase (Fig. 3), as was the case in a previous analysis of a forced ocean model (Mongwe et al., 2016).

In addition to increasing CO_2 solubility, the rapid cooling at the onset of autumn also deepens the MLD (March–June, Fig. 7), which induces entrainment of DIC, increasing surface CO_2 concentration and weakening the ocean–atmosphere gradient and, in some instances, reversing the air–sea flux to out-gassing (Lenton et al., 2013a; Mahadevan et al., 2011; Metzl et al., 2006). While these processes (cooling and DIC entrainment) are likely to co-occur in the Southern Ocean, in CMIP5 models they are characterized by their extremes: temperature impact of solubility exceeds the rate of entrainment (Figs. 6, 10). Because of the dominance of the solubility effect in group-SST models, the impact of DIC entrainment on surface $p\text{CO}_2$ changes, the weakening of CO_2 in-gassing/out-gassing only happens in mid–late winter (June–July–August), when entrainment fluxes peak (Fig. 10) and the SST rate approaches zero (Fig. 5).

In the spring–summer transition, primary production is expected to enhance the net CO_2 uptake (Thomalla et al., 2011; Le Quééré and Saltzman, 2013). However, the elevated surface warming rates during spring reduces CO_2 solubility in group-SST models and overwhelms the role of primary production in the seasonal cycle of $p\text{CO}_2$ and $F\text{CO}_2$ (atmospheric CO_2 uptake). As a consequence, these group-SST models mostly show a constant or weakening net CO_2 uptake flux during spring in the Pacific and Atlantic basins even though primary production is occurring and is relatively elevated (Fig. 3, 8). Though some models show chlorophyll concentrations comparable to observations (e.g., GFDL-ESM2M, CNRM-CM5, CanESM2), and sometimes greater (e.g., MRI-ESM), the impact of temperature-driven solubility still dominates due to the phasing of the rates of the two drivers (Fig. 2a–c). The Indian Basin, however, shows the only exception to this phenomenon. Here, the amplitude of the seasonal surface warming is relatively smaller ($\sim 0.5^\circ\text{C}^{-1}\text{ month}^{-1}$ lower than the Pacific and Atlantic basins), and the biologically driven CO_2 uptake becomes notable and shows a net strengthening of the sink of CO_2 during spring (Fig. 3c).

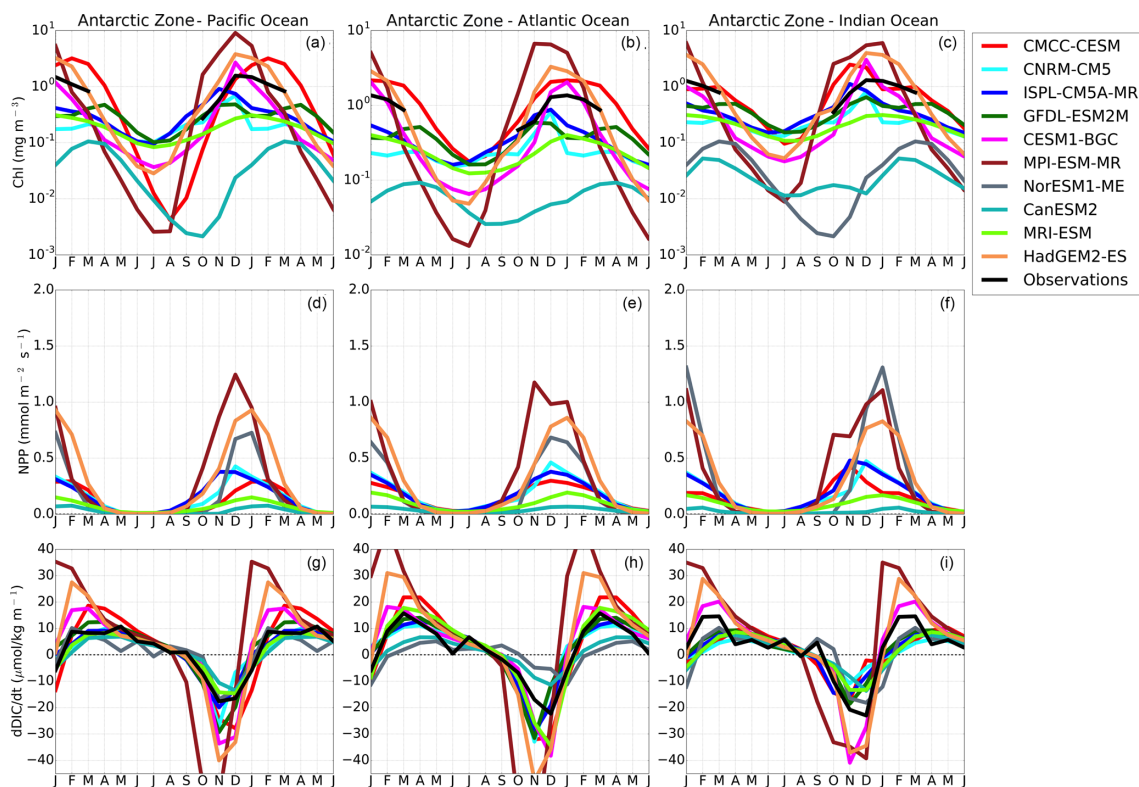


Figure 9. Same as Fig. 8 for the Antarctic Zone.

Though almost all analyzed CMIP5 models (with the exception of NorESM1-ME) exaggerate the warming and cooling rates in autumn and spring, group-DIC models do not manifest the expected temperature-driven solubility impact on $p\text{CO}_2$ and $F\text{CO}_2$ (Fig. 2). Instead, the seasonal cycles of $p\text{CO}_2$ and $F\text{CO}_2$ are controlled by DIC changes, which are driven by an overestimated seasonal primary production and the associated export carbon (Fig. 8). It is striking how in these models the seasonal cycle of chlorophyll and $F\text{CO}_2$ are in phase (Fig. 3a–c, 8a–c, with linear correlation coefficients always larger than 0.9 not shown) but, as we discuss below, this is not because the temperature rates of change are correctly scaled but because the biogeochemical process rates are exaggerated (Fig. 8).

Because of the particularly enhanced production in group-DIC models, the CO_2 sink is stronger (Fig. 8) with respect to observation estimates during spring. This is visible in the reduction of surface DIC (negative $d\text{DIC}/dt$ in Fig. 8a, g–i), which can only be explained by drawdown due to the formation and export of organic matter (Le Quéré and Saltzman, 2013). However, note that in the same way, after the December production peak, both CMIP5 models and observations show an increase in surface DIC concentrations (positive $d\text{DIC}/dt$) until March (Fig. 8g–i). These DIC growth rates are particularly enhanced in group-DIC models compared to some group-SST and observations (Fig. S9). The

onset of these DIC increases also coincides with the depletion of surface oxygen (Fig. S9), which we speculate is due to the remineralization of organic matter to DIC through respiration. Unfortunately, only a few models have stored the respiration rates; therefore the full reason for this DIC rebound remains to be examined at a later stage. We would, however, tend to exclude other processes, because the onset of CO_2 out-gassing seen in March in group-DIC models occurs prior to significant MLD deepening (Fig. 7) and entrainment fluxes; therefore remineralization is likely be a key process here (Fig. 8).

4.2 Antarctic Zone (AZ)

The seasonal cycle framework summarized in Fig. 6 shows that the variability of $F\text{CO}_2$ and $p\text{CO}_2$ in the Landschützer et al. (2014) product is characterized by a stronger DIC control (annual mean $M_{T-\text{DIC}} < -2$) relative to the Sub-Antarctic ($M_{T-\text{DIC}} \approx -1$), except in the spring season ($M_{T-\text{DIC}} = 1$). This DIC control is spatially uniform in the Antarctic Zone across all three basins (Fig. 4). The available datasets indicate that the combination of weaker SST rates due to lower solar heating fluxes (Fig. 5), and stronger shallower vertical DIC maxima (Fig. 10) favor a stronger DIC control through larger surface DIC rates. The spatial uniformity in the seasonality of $F\text{CO}_2$ is also evident in the satellite chlorophyll and calculated $d\text{DIC}/dt$ from GLODAP2 in Fig. 9. Contrary to the

Sub-Antarctic this might be suggesting that FCO_2 mechanisms here are less local. It could be hypothesized that the seasonal extent of sea ice, deeper mixing and heat balance differences affect this region more uniformly compared to the Sub-Antarctic Zone, and hence the mechanisms of FCO_2 are spatially homogeneous. However, we cannot forget that sparseness of observations in this region is a key limitation to data products (Bakker et al., 2014; Gregor et al., 2017; Monteiro et al., 2010; Rödenbeck et al., 2013) that might hamper the emergence of basin-specific features. Consequently, this highlights the importance and need to prioritize independent observations in the Southern Ocean south of the polar front and in the marginal ice zone. Increased observational efforts should also include a variety of platforms such as autonomous vehicles like gliders (Monteiro et al., 2015) and biogeochemical floats (Johnson et al., 2017) in addition to ongoing ship-based measurements.

In general terms, CMIP5 models are mostly in agreement (with an exception of MRI-ESM) with the observational product on the dominant role of DIC to regulating the seasonal cycle of FCO_2 (Fig. 6d–f), though not all models agree in the phase of the seasonal cycle of FCO_2 (e.g., CanESM2, Fig. 2). Though CMIP5 models still mostly show the SST rates biases in autumn and spring with respect to observed estimates, the stronger and near-surface vertical DIC maxima (Fig. 10) likely favor DIC as a dominant driver of FCO_2 changes. Differences between group-SST and group-DIC models are only evident in mid-summer, when SST rates heighten and primary production peaks (Fig. 3, 9). Probably because of sea ice presence, the onset of SST warming is a month later (November) here in comparison to the Sub-Antarctic (October). This subsequently allows the onset of primary production before the surface warming, which then permits the biological CO_2 uptake to be notable in group-SST models. Thus the two model groups here agree in the FCO_2 in-gassing during spring with group-SST models being the closest to the observational product. The MRI-ESM is the only model showing anomalous solubility dominance during autumn and spring as in the Sub-Antarctic Zone.

This coherence of CMIP5 models and observations in the Antarctic Zone may suggest that CMIP5 models compare better to observations in this region (Fig. 4). However, because CMIP5 models also show this spatial homogeneity in the Sub-Antarctic Zone (contrary to observational estimates), it is not clear whether this indicates an improved skill in CMIP5 model to the mechanisms of FCO_2 in this region, or whether both CMIP5 models and the observational product lack spatial sensitivity to the drivers of FCO_2 . The sparseness of observations in the AZ points to the latter.

The cause of differences in the seasonal rates of SST change in group-SST models remains a subject of ongoing research. The Southern Ocean is a part of the global ocean (upwelling), where Earth systems models show a persistent warming SST bias (Hirahara et al., 2014). Several studies highlight potential explanations, but the main reasons re-

main uncertain. For example, CMIP5 model differences in the magnitude and meridional location of the peak of wind speeds in the Southern Ocean (Bracegirdle et al., 2013) and MLD differences (Meijers, 2014; Sallée et al., 2013) may be such that the net effect of change on surface turbulence and mixing leads to these amplified surface temperature rates. Other known CMIP5 models' biases that may contribute includes heat fluxes and storage (Frölicher et al., 2015) as well as sea-ice dynamics (Turner et al., 2013). Notwithstanding these, investigation of the reasons for sources of these dSST/dt biases is out of the scope of this study. Our aim here is to show that understanding biases in the drivers of $p\text{CO}_2$ (DIC and SST) at the seasonal scale is necessary to understand differences in the seasonal cycle of FCO_2 between models and observational products. However, we recommend that the mechanistic basis for the differences in the seasonal rates of warming and cooling be urgently investigated further

5 Synthesis

We used a seasonal cycle framework to highlight and examine two major biases in respect of $p\text{CO}_2$ and FCO_2 in 10 CMIP5 models in the Southern Ocean.

Firstly, we examined the general exaggeration of the seasonal rates of change of SST in autumn and spring seasons during peak cooling and warming, respectively, with respect to available observations. These elevated rates of SST change tip the control of the seasonal cycle of $p\text{CO}_2$ and FCO_2 towards SST from DIC and result in a divergence between the observed and modeled seasonal cycles, particularly in the Sub-Antarctic Zone. While almost all analyzed models (9 of 10) show these SST-driven biases, 3 of the 10 (namely NorESM1-ME, HadGEM-ES and MPI-ESM) do not show these solubility biases because of their overly exaggerated primary production (and remineralization) rates such that biologically driven DIC changes mainly regulate the seasonal cycle of FCO_2 . These models reproduce the observed phasing of FCO_2 as a result of an incorrect scaling of the biogeochemical fluxes. In the Antarctic Zone, CMIP5 models compare better with observations relative to the Sub-Antarctic Zone. This is mostly because both CMIP5 models and observational product estimates show a spatial and temporal uniformity in the characteristics of FCO_2 in the Antarctic Zone. However, it is not certain if this is because model process dynamics perform better in this high-latitude zone or that the observational products variability is itself limited by the lack of in situ data. This remains an open question that needs to be explored further and highlights the need for increased scale-sensitive and independent observations south of the PF and into the sea-ice zone.

The second major bias is that contrary to observational products estimates, CMIP5 models generally show an equal sensitivity to basin-scale FCO_2 drivers (except for CMCC-

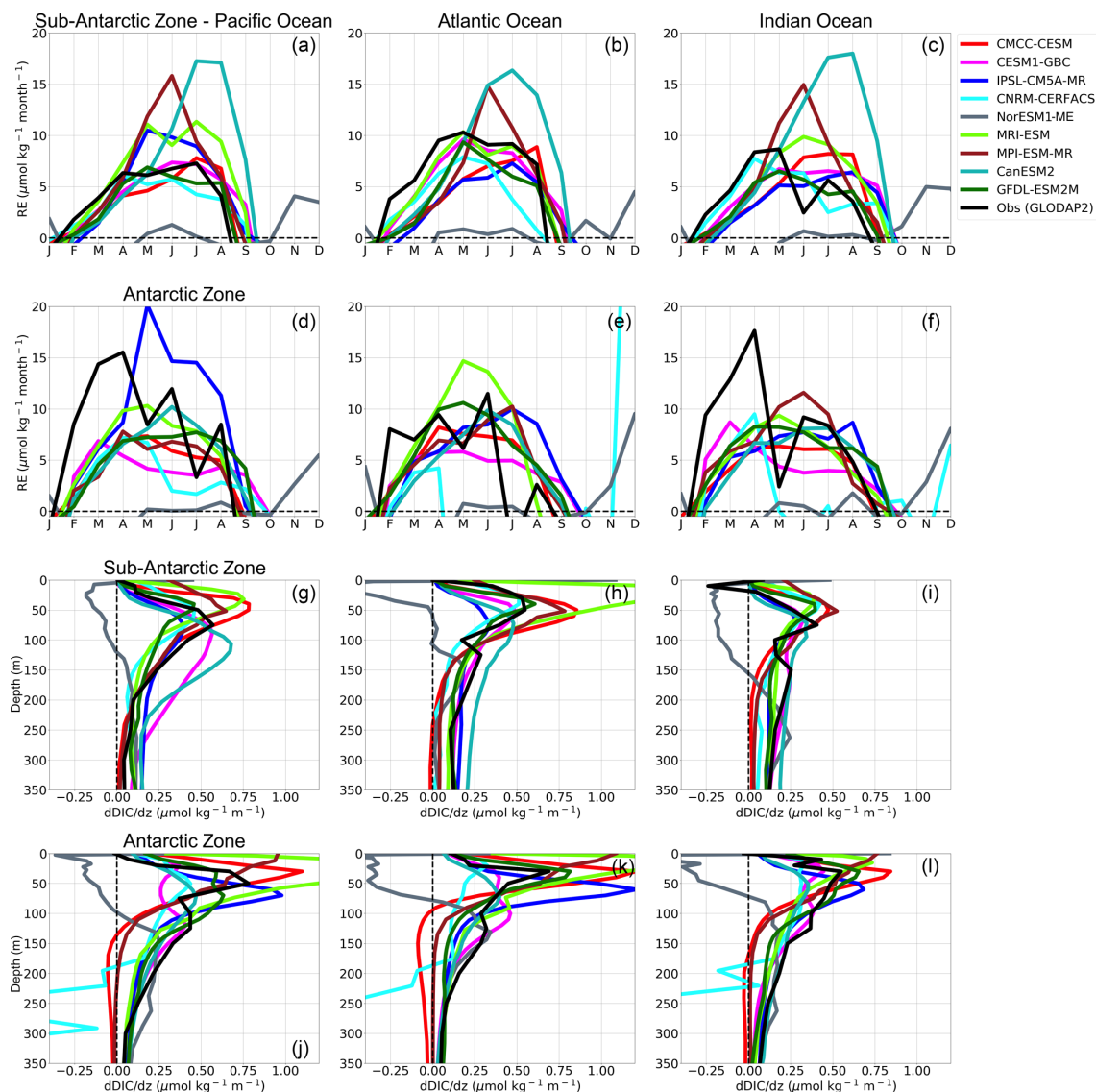


Figure 10. (a–f) Estimated DIC entrainment fluxes (mol kg month^{-1}) at the base of the mixed layer and (g–i) vertical DIC gradients ($\mu\text{mol kg}^{-1} \text{m}^{-1}$) in the Sub-Antarctic and Antarctic zones of the Pacific Ocean (first column), Atlantic Ocean (second column) and Indian Ocean (third column).

ESM, GFDL-ESM2M and CESM1-BGC) and hence the seasonal cycle of $F\text{CO}_2$ has similar phasing in all three basins of the Sub-Antarctic Zone. This is in contrast to observational and remote sensing products that highlight strong seasonal and interannually varying basin contrasts in both $p\text{CO}_2$ and phytoplankton biomass. It is not clear if this is due to inadequate carbon process parameterization or improper representation of the dynamics of the physics. This should be investigated further with CMIP6 models, and our analysis framework is proposed as a useful tool to diagnose the dominant drivers. Contrary to observed estimates, CMIP5 models simulate $F\text{CO}_2$ seasonal dynamics that are zonally homogeneous, and we suggest that any investigation of local (basin-scale) mechanisms, dynamics and long-term trends of $F\text{CO}_2$

using CMIP5 models must remain tentative and should be treated with caution. This highlights a key area of development for the next generation of models such as those planned to be used for CMIP6.

Data availability. The data used in the analysis can be obtained from the following sources. CMIP5 data: <https://esgf-data.dkrz.de/search/cmip5-dkrz/> (Taylor et al., 2012) (last access: March 2017). $F\text{CO}_2$ and $p\text{CO}_2$ data product: Landschützer, et al. (2014), http://cdiac.ornl.gov/ftp/oceans/spco2_1982_2011_ETH_SOM-FFN, (last access: March 2017). $p\text{CO}_2$ data estimates: Takahashi et al. (2009), http://www.ldeo.columbia.edu/res/pi/CO2/carbondioxide/pages/air_sea_flux_2000.html (last ac-

cess: January 2015). $p\text{CO}_2$ data product: Groger et al. (2017), https://figshare.com/articles/_/5369038. MLD: de Boyer Montégut et al. (2004) (last access: November 2017). http://www.ifremer.fr/cerweb/deboyer/mld/Surface_Mixed_Layer_Depth.php. Sea surface temperature and sea surface salinity: Word Atlas data version version (WOA3) (last access: January 2015). Satellite chlorophyll: Johnson et al. (2013), <http://oceancolor.gsfc.nasa.gov/> (last access: February 2016).

Supplement. The supplement related to this article is available online at: <https://doi.org/10.5194/bg-15-2851-2018-supplement>.

Competing interests. The authors declare that they have no conflict of interest.

Special issue statement. This article is part of the special issue “The 10th International Carbon Dioxide Conference (ICDC10) and the 19th WMO/IAEA Meeting on Carbon Dioxide, other Greenhouse Gases and Related Measurement Techniques (GGMT-2017) (AMT/ACP/BG/CP/ESD inter-journal SI)”. It is a result of the 10th International Carbon Dioxide Conference, Interlaken, Switzerland, 21–25 August 2017.

Acknowledgements. This work was undertaken with financial support from the following South African institutions: CSIR Parliamentary Grant, National Research Foundation (NRF SANAP programme), Department of Science and Technology South Africa (DST), and the Applied Centre for Climate and Earth Systems Science (ACCESS). We thank the CSIR Centre for High Performance Computing (CHPC) for providing the resources for doing this analysis. We also want to thank the CMIP5 model community, Peter Landschützer, Taro Takahashi and Luke Gregor for making their products available as well as the three reviewers for their productive comments that we think have strengthened the paper.

Edited by: Katja Fennel

Reviewed by: three anonymous referees

References

- Adachi, Y., Yukimoto, S., Deushi, M., Obata, A., Nakano, H., Tanaka, T. Y., Hosaka, M., Sakami, T., Yoshimura, H., Hirabara, M., Shindo, E., Tsujino, H., Mizuta, R., Yabu, S., Koshiro, T., Ose, T., and Kitoh, A.: Basic performance of a new earth system model of the Meteorological Research Institute, *Pap. Meteorol. Geophys.*, 64, 1–19, <https://doi.org/10.2467/mripapers.64.1>, 2013.
- Anav, A., Friedlingstein, P., Kidston, M., Bopp, L., Ciais, P., Cox, P., Jones, C., Jung, M., Myneni, R., and Zhu, Z.: Evaluating the land and ocean components of the global carbon cycle in the CMIP5 earth system models, *J. Climate*, 26, 6801–6843, <https://doi.org/10.1175/JCLI-D-12-00417.1>, 2013.
- Bakker, D. C. E., Pfeil, B., Smith, K., Hankin, S., Olsen, A., Alin, S. R., Cosca, C., Harasawa, S., Kozyr, A., Nojiri, Y., O'Brien, K. M., Schuster, U., Telszewski, M., Tilbrook, B., Wada, C., Akl, J., Barbero, L., Bates, N. R., Boutin, J., Bozec, Y., Cai, W.-J., Castle, R. D., Chavez, F. P., Chen, L., Chierici, M., Currie, K., de Baar, H. J. W., Evans, W., Feely, R. A., Fransson, A., Gao, Z., Hales, B., Hardman-Mountford, N. J., Hoppema, M., Huang, W.-J., Hunt, C. W., Huss, B., Ichikawa, T., Johannessen, T., Jones, E. M., Jones, S. D., Jutterström, S., Kitidis, V., Körtzinger, A., Landschützer, P., Lauvset, S. K., Lefèvre, N., Manke, A. B., Mathis, J. T., Merlivat, L., Metzl, N., Murata, A., Newberger, T., Omar, A. M., Ono, T., Park, G.-H., Pater-son, K., Pierrot, D., Ríos, A. F., Sabine, C. L., Saito, S., Salis-bury, J., Sarma, V. V. S. S., Schlitzer, R., Sieger, R., Skjelvan, I., Steinhoff, T., Sullivan, K. F., Sun, H., Sutton, A. J., Suzuki, T., Sweeney, C., Takahashi, T., Tjiputra, J., Tsurushima, N., van Heuven, S. M. A. C., Vandemark, D., Vlahos, P., Wallace, D. W. R., Wanninkhof, R., and Watson, A. J.: An update to the Surface Ocean CO_2 Atlas (SOCAT version 2), *Earth Syst. Sci. Data*, 6, 69–90, <https://doi.org/10.5194/essd-6-69-2014>, 2014.
- Barbero, L., Boutin, J., Merlivat, L., Martin, N., Takahashi, T., Sutherland, S. C., and Wanninkhof, R.: Importance of water mass formation regions for the air-sea CO_2 flux estimate in the southern ocean, *Glob. Biogeochem. Cy.*, 25, 1–16, <https://doi.org/10.1029/2010GB003818>, 2011.
- Boyd, P. W. and Ellwood, M. J.: The biogeochemical cycle of iron in the ocean, *Nat. Geosci.*, 3, 675–682, <https://doi.org/10.1038/ngeo964>, 2010.
- Bracegirdle, T. J., Shuckburgh, E., Sallee, J. B., Wang, Z., Meijers, A. J. S., Bruneau, N., Phillips, T., and Wilcox, L. J.: Assessment of surface winds over the atlantic, indian, and pacific ocean sectors of the southern ocean in cmip5 models: Historical bias, forcing response, and state dependence, *J. Geophys. Res. Atmos.*, 118, 547–562, <https://doi.org/10.1002/jgrd.50153>, 2013.
- de Boyer Montégut, C., Madec, G., Fischer, A. S., Lazar, A., and Iudicone, D.: Mixed layer depth over the global ocean: An examination of profile data and a profile-based climatology, *J. Geophys. Res.-Ocean*, 109, 1–20, <https://doi.org/10.1029/2004JC002378>, 2004.
- Dickson, A. G. and Millero, F. J.: A comparison of the equilibrium constants for the dissociation of carbonic acid in seawater media, *Deep Sea Res. Pt. A, Oceanogr. Res. Pap.*, 34, 1733–1743, [https://doi.org/10.1016/0198-0149\(87\)90021-5](https://doi.org/10.1016/0198-0149(87)90021-5), 1987.
- Dufour, C. O., Sommer, J. Le, Gehlen, M., Orr, J. C., Molines, J. M., Simeon, J. and Barnier, B.: Eddy compensation and controls of the enhanced sea-to-air CO_2 flux during positive phases of the Southern Annular Mode, *Glob. Biogeochem. Cy.*, 27, 950–961, <https://doi.org/10.1002/gbc.20090>, 2013.
- du Plessis, M., Swart, S., Anson, I. J., and Mahadevan, A.: Submesoscale processes promote seasonal restratification in the Subantarctic Ocean, *J. Geophys. Res. Ocean.*, 122, 2960–2975, <https://doi.org/10.1002/2016JC012494>, 2017.
- Dunne, J. P., John, J. G., Shevliakova, S., Stouffer, R. J., Krasting, J. P., Malyshev, S. L., Milly, P. C. D., Sentman, L. T., Adcroft, A. J., Cooke, W., Dunne, K. A., Griffies, S. M., Hallberg, R. W., Harrison, M. J., Levy, H., Wittenberg, A. T., Phillips, P. J., and Zadeh, N.: GFDL's ESM2 global coupled climate-carbon earth system models, Part II: Carbon system formulation and

- baseline simulation characteristics, *J. Climate*, 26, 2247–2267, doi:10.1175/JCLI-D-12-00150.1, 2013.
- Feely, R. A., Wanninkhof, R., McGillis, W., Carr M. E., and Cosca, C.: Effects of wind speed and gas exchange parameterizations on the air-sea CO_2 fluxes in the equatorial Pacific Ocean, *J. Geophys. Res.*, 109, C08S03, https://doi.org/10.1029/2003JC001896, 2004.
- Frölicher, T. L., Sarmiento, J. L., Paynter, D. J., Dunne, J. P., Krasting, J. P., and Winton, M.: Dominance of the Southern Ocean in anthropogenic carbon and heat uptake in CMIP5 models, *J. Climate*, 28, 862–886, https://doi.org/10.1175/JCLI-D-14-00117.1, 2015.
- Fung, I. Y., Doney, S. C., Lindsay, K., and John, J.: Evolution of carbon sinks in a changing climate, *Proc. Natl. Acad. Sci.*, 102, 11201–11206, https://doi.org/10.1073/pnas.0504949102, 2005.
- Graham, R. M., De Boer, A. M., van Sebille, E., Kohfeld, K. E., and Schlosser, C.: Inferring source regions and supply mechanisms of iron in the Southern Ocean from satellite chlorophyll data, *Deep. Res. Pt. I*, 104, 9–25, https://doi.org/10.1016/j.dsr.2015.05.007, 2015.
- Gregor, L., Kok, S., and Monteiro, P. M. S.: Empirical methods for the estimation of Southern Ocean CO_2 : support vector and random forest regression, *Biogeosciences*, 14, 5551–5569, https://doi.org/10.5194/bg-14-5551-2017, 2017.
- Gregor, L., Kok, S., and Monteiro, P. M. S.: Interannual drivers of the seasonal cycle of CO_2 in the Southern Ocean, *Biogeosciences*, 15, 2361–2378, https://doi.org/10.5194/bg-15-2361-2018, 2018.
- Gruber, N., Gloor, M., Mikaloff Fletcher, S. E., Doney, S. C., Dutkiewicz, S., Follows, M. J., Gerber, M., Jacobson, A. R., Joos, F., Lindsay, K., Menemenlis, D., Mouchet, A., Müller, S. A., Sarmiento, J. L., and Takahashi, T.: Oceanic sources, sinks, and transport of atmospheric CO_2 , *Glob. Biogeochem. Cy.*, 23, 1–21, https://doi.org/10.1029/2008GB003349, 2009.
- Hauck, J. and Völker, C.: A multi-model study on the Southern Ocean CO_2 uptake and the role of the biological carbon pump in the 21st century, *EGU Gen. Assem.*, 17, 12225, https://doi.org/10.1002/2015GB005140, 2015.
- Hauck, J., Völker, C., Wolf-Gladrow, D. a., Laufkötter, C., Vogt, M., Aumont, O., Bopp, L., Buitenhuis, E. T., Doney, S. C., Dunne, J., Gruber, N., John, J., Le Quééré, C., Lima, I. D., Nakano, H., and Totterdell, I.: On the Southern Ocean CO_2 uptake and the role of the biological carbon pump in the 21st century, *Glob. Biogeochem. Cy.*, 29, 1451–1470, https://doi.org/10.1002/2015GB005140, 2015.
- Hirahara, S., Ishii, M., and Fukuda, Y.: Centennial-scale sea surface temperature analysis and its uncertainty, *J. Climate*, 27, 57–75, https://doi.org/10.1175/JCLI-D-12-00837.1, 2014.
- Ilyina, T., Six, K. D., Segsneider, J., Maier-Reimer, E., Li, H., and Núñez-Riboni, I.: Global ocean biogeochemistry model HAMOCC: Model architecture and performance as component of the MPI-Earth system model in different CMIP5 experimental realizations, *J. Adv. Model. Earth Syst.*, 5, 287–315, https://doi.org/10.1029/2012MS000178, 2013.
- Johnson, K. S., Plant, J. N., Coletti, L. J., Jannasch, H. W., Sakamoto, C. M., Riser, S. C., Swift, D. D., Williams, N. L., Boss, E., Haëntjens, N., Talley, L. D., and Sarmiento, J. L.: Biogeochemical sensor performance in the SOCOM profiling float array, *J. Geophys. Res.-Ocean*, https://doi.org/10.1002/2017JC012838, 2017.
- Johnson, R., Strutton, P. G., Wright, S. W., McMinn, A., and Meiners, K. M.: Three improved satellite chlorophyll algorithms for the Southern Ocean, *J. Geophys. Res.-Ocean.*, 118, 3694–3703, https://doi.org/10.1002/jgrc.20270, 2013.
- Kessler, A. and Tjiputra, J.: The Southern Ocean as a constraint to reduce uncertainty in future ocean carbon sinks, *Earth Syst. Dynam.*, 7, 295–312, https://doi.org/10.5194/esd-7-295-2016, 2016.
- Landschützer, P., Gruber, N., and Bakker, D. C. E. Stemmler, I., and Six, K. D.: Strengthening seasonal marine CO_2 variations due to increasing atmospheric CO_2 , *Nat. Clim. Change*, 8, 146–150, https://doi.org/10.1038/s41558-017-0057-x, 2018.
- Landschützer, P., Gruber, N., and Bakker, D. C. E.: Decadal variations and trends of the global ocean carbon sink, *Glob. Biogeochem. Cy.*, 30, 1396–1417, https://doi.org/10.1002/2015GB005359, 2016.
- Landschützer, P., Gruber, N., Haumann, F. A., Rodenbeck, C., Bakker, D. C. E., van Heuven, S., Hoppema, M., Metzl, N., Sweeney, C., Takahashi, T., Tilbrook, B., and Wanninkhof, R.: The reinvigoration of the Southern Ocean carbon sink, *Science*, 349, 1221–1224, https://doi.org/10.1126/science.aab2620, 2015.
- Landschützer, P., Gruber, N., Bakker, D. C. E., and Schuster, U.: Recent variability of the global ocean carbon sink, *Glob. Planet. Change*, 927–949, https://doi.org/10.1002/2014GB004853, 2014.
- Landschützer, P., Gruber, N., Bakker, D. C. E., Schuster, U., Nakaoka, S., Payne, M. R., Sasse, T. P., and Zeng, J.: A neural network-based estimate of the seasonal to inter-annual variability of the Atlantic Ocean carbon sink, *Biogeosciences*, 10, 7793–7815, https://doi.org/10.5194/bg-10-7793-2013, 2013.
- Lauvset, S. K., Key, R. M., Olsen, A., van Heuven, S., Velo, A., Lin, X., Schirnick, C., Kozyr, A., Tanhua, T., Hoppema, M., Jutterström, S., Steinfeldt, R., Jeansson, E., Ishii, M., Perez, F. F., Suzuki, T., and Watelet, S.: A new global interior ocean mapped climatology: the $1^\circ \times 1^\circ$ GLODAP version 2, *Earth Syst. Sci. Data*, 8, 325–340, https://doi.org/10.5194/essd-8-325-2016, 2016.
- Lee, K., Tong, L. T., Millero, F. J., Sabine, C. L., Dickson, A. G., Goyet, C., Park, G. H., Wanninkhof, R., Feely, R. A., and Key, R. M.: Global relationships of total alkalinity with salinity and temperature in surface waters of the world's oceans, *Geophys. Res. Lett.*, 33, 1–5, https://doi.org/10.1029/2006GL027207, 2006.
- Lenton, A., Metzl, N., Takahashi, T., Kuchinke, M., Matear, R. J., Roy, T., Sutherland, S. C., Sweeney, C., and Tilbrook, B.: The observed evolution of oceanic $p\text{CO}_2$ and its drivers over the last two decades, *Glob. Biogeochem. Cy.*, 26, 1–14, https://doi.org/10.1029/2011GB004095, 2012.
- Lenton, A., Tilbrook, B., Law, R. M., Bakker, D., Doney, S. C., Gruber, N., Ishii, M., Hoppema, M., Lovenduski, N. S., Matear, R. J., McNeil, B. I., Metzl, N., Mikaloff Fletcher, S. E., Monteiro, P. M. S., Rödenbeck, C., Sweeney, C., and Takahashi, T.: Sea-air CO_2 fluxes in the Southern Ocean for the period 1990–2009, *Biogeosciences*, 10, 4037–4054, https://doi.org/10.5194/bg-10-4037-2013, 2013.
- Le Quééré, C. and Saltzman, E. S.: Surface Ocean-Lower Atmosphere Processes, *Geophysical Monograph Series*, https://doi.org/10.1029/GM187, 2013.

- Le Quéré, C., Rödenbeck, C., Buitenhuis, E. T., Conway, T. J., Langenfelds, R., Gomez, A., Labuschagne, C., Ramonet, M., Nakazawa, T., Metzl, N., Gillett, N., and Heimann, M.: Saturation of the southern ocean CO_2 sink due to recent climate change, *Science*, 316, 1735–1738, <https://doi.org/10.1126/science.1136188>, 2007.
- Le Quéré, C., Andrew, R. M., Canadell, J. G., Sitch, S., Korsbakken, J. I., Peters, G. P., Manning, A. C., Boden, T. A., Tans, P. P., Houghton, R. A., Keeling, R. F., Alin, S., Andrews, O. D., Anthoni, P., Barbero, L., Bopp, L., Chevallier, F., Chini, L. P., Ciais, P., Currie, K., Delire, C., Doney, S. C., Friedlingstein, P., Gkritzalis, T., Harris, I., Hauck, J., Haverd, V., Hoppema, M., Klein Goldewijk, K., Jain, A. K., Kato, E., Körtzinger, A., Landschützer, P., Lefèvre, N., Lenton, A., Lienert, S., Lombardozi, D., Melton, J. R., Metzl, N., Millero, F., Monteiro, P. M. S., Munro, D. R., Nabel, J. E. M. S., Nakaoka, S.-I., O'Brien, K., Olsen, A., Omar, A. M., Ono, T., Pierrot, D., Poulter, B., Rödenbeck, C., Salisbury, J., Schuster, U., Schwinger, J., Séférian, R., Skjelvan, I., Stocker, B. D., Sutton, A. J., Takahashi, T., Tian, H., Tilbrook, B., van der Laan-Luijckx, I. T., van der Werf, G. R., Viovy, N., Walker, A. P., Wiltshire, A. J., and Zaehle, S.: Global Carbon Budget 2016, *Earth Syst. Sci. Data*, 8, 605–649, <https://doi.org/10.5194/essd-8-605-2016>, 2016.
- Leung, S., Cabré, A., and Marinov, I.: A latitudinally banded phytoplankton response to 21st century climate change in the Southern Ocean across the CMIP5 model suite, *Biogeosciences*, 12, 5715–5734, <https://doi.org/10.5194/bg-12-5715-2015>, 2015.
- Locarnini, R. A., Mishonov, A. V., Antonov, J. I., Boyer, T. P., Garcia, H. E., Baranova, O. K., Zweng, M. M., Paver, C. R., Reagan, J. R., Johnson, D. R., Hamilton, M., and Seidov, D.: World Ocean Atlas 2013, Vol. 1, Temperature, 2013.
- Mahadevan, A., Tagliabue, A., Bopp, L., Lenton, A., Memery, L., and Levy, M.: Impact of episodic vertical fluxes on sea surface $p\text{CO}_2$, *Philos. Tr. R. Soc. S.-A.*, 369, 2009–2025, <https://doi.org/10.1098/rsta.2010.0340>, 2011.
- Mahadevan, A., D'Asaro, E., Lee, C. and Perry, M. J.: Eddy-driven stratification initiates North Atlantic spring phytoplankton blooms, *Science*, 80, 54–58, <https://doi.org/10.1126/science.1218740>, 2012.
- Marinov, I. and Gnanadesikan, A.: Changes in ocean circulation and carbon storage are decoupled from air-sea CO_2 fluxes, *Biogeosciences*, 8, 505–513, <https://doi.org/10.5194/bg-8-505-2011>, 2011.
- Marinov, I., Gnanadesikan, A., Toggweiler, J. R., and Sarmiento, J. L.: The Southern Ocean biogeochemical divide, *Nature*, 441, 964–967, <https://doi.org/10.1038/nature04883>, 2006.
- Matear, R. J. and Lenton, A.: Impact of Historical Climate Change on the Southern Ocean Carbon Cycle, *J. Climate*, 21, 5820–5834, <https://doi.org/10.1175/2008JCLI2194.1>, 2008.
- McNeil, B. I., Metzl, N., Key, R. M., Matear, R. J., and Corbiere, A.: An empirical estimate of the Southern Ocean air-sea CO_2 flux, *Glob. Biogeochem. Cy.*, 21, 1–16, <https://doi.org/10.1029/2007GB002991>, 2007.
- Mehrbach, C., Culbertson, C. H., Hawley, J. E., and Pytkowicz, R. M.: Measurement of the Apparent Dissociation Constants of Carbonic Acid in Seawater At Atmospheric Pressure, *Limnol. Ocean.*, 18, 897–907, <https://doi.org/10.4319/lo.1973.18.6.0897>, 1973.
- Metzl, N.: Decadal increase of oceanic carbon dioxide in Southern Indian Ocean surface waters (1991–2007), *Deep. Res. Pt. II*, 56, 607–619, <https://doi.org/10.1016/j.dsr2.2008.12.007>, 2009.
- Metzl, N., Brunet, C., Jabaud-Jan, A., Poisson, A., and Schauer, B.: Summer and winter air-sea CO_2 fluxes in the Southern Ocean, *Deep. Res. Pt. I*, 53, 1548–1563, <https://doi.org/10.1016/j.dsr.2006.07.006>, 2006.
- Mongwe, N. P., Chang, N., and Monteiro, P. M. S.: The seasonal cycle as a mode to diagnose biases in modelled CO_2 fluxes in the Southern Ocean, *Ocean Model.*, 106, 90–103, <https://doi.org/10.1016/j.ocemod.2016.09.006>, 2016.
- Monteiro, P., Schuster, U., Hood, M., Lenton, A., Metzl, N., Olsen, A., Rogers, K., Sabine, C., Takahashi, T., Tilbrook, B., Yoder, J., Wanninkhof, R., Watson, A.: A global sea surface carbon observing system: Assessment of changing sea surface CO_2 and air-sea CO_2 fluxes, in: Proceedings of the “OceanObs’09: Sustained Ocean Observations and Information for Society” edited by: Hall, J. and Harrison, D. E., Stammer, D., ESA Publ. WPP-306, Venice, Italy, <https://doi.org/10.5270/OceanObs09.cwp.64>, 21–25 SeptConference, 2010.
- Monteiro, P. M. S., Gregor, L., Lévy, M., Maenner, S., Sabine, C. L., and Swart, S.: Intra-seasonal variability linked to sampling alias in air – sea CO_2 fluxes in the Southern Ocean, *Geophys. Res. Lett.*, 1–8, <https://doi.org/10.1002/2015GL066009>, 2015.
- Moore, J. K., Doney, S. C., and Lindsay, K.: Upper ocean ecosystem dynamics and iron cycling in a global three-dimensional model, *Glob. Biogeochem. Cy.*, 18, 1–21, <https://doi.org/10.1029/2004GB002220>, 2004.
- Orsi, A. H., Whitworth, T., and Nowlin, W. D.: On the meridional extent and fronts of the Antarctic Circumpolar Current, *Deep. Res. Pt. I*, 42, 641–673, [https://doi.org/10.1016/0967-0637\(95\)00021-W](https://doi.org/10.1016/0967-0637(95)00021-W), 1995.
- Pasquer, B., Metzl, N., Goosse, H., and Lancelot, C.: What drives the seasonality of air-sea CO_2 fluxes in the ice-free zone of the Southern Ocean: A 1D coupled physical-biogeochemical model approach, *Mar. Chem.*, 177, 554–565, <https://doi.org/10.1016/j.marchem.2015.08.008>, 2015.
- Palmer, J. R. and Totterdell, I. J.: Production and export in a global ocean ecosystem model, *Deep. Res. Pt. I*, 48, 1169–1198, [doi:10.1016/S0967-0637\(00\)00080-7](https://doi.org/10.1016/S0967-0637(00)00080-7), 2001.
- Pierrot, D., Lewis, E., and Wallace, D. W. R.: MS Excel Program Developed for CO_2 System Calculations. ORNL/CDIAC-105a, Carbon Dioxide Information Analysis Center, Oak Ridge National Laboratory, U.S. Department of Energy, Oak Ridge, Tennessee, https://doi.org/10.3334/CDIAC/otg.CO2SYS_XLS_CDIAC105a, 2006.
- Ritter, R., Landschützer, P., Gruber, N., Fay, A. R., Iida, Y., Jones, S., Nakaoka, S., Park, G. H., Peylin, P., Rödenbeck, C., Rodgers, K. B., Shutler, J. D., and Zeng, J.: Observation-Based Trends of the Southern Ocean Carbon Sink, *Geophys. Res. Lett.*, <https://doi.org/10.1002/2017GL074837>, 2017.
- Rödenbeck, C., Keeling, R. F., Bakker, D. C. E., Metzl, N., Olsen, A., Sabine, C., and Heimann, M.: Global surface-ocean $p\text{CO}_2$ and sea-air CO_2 flux variability from an observation-driven ocean mixed-layer scheme, *Ocean Sci.*, 9, 193–216, <https://doi.org/10.5194/os-9-193-2013>, 2013.
- Rödenbeck, C., Bakker, D. C. E., Gruber, N., Iida, Y., Jacobson, A. R., Jones, S., Landschützer, P., Metzl, N., Nakaoka,

- S., Olsen, A., Park, G.-H., Peylin, P., Rodgers, K. B., Sasse, T. P., Schuster, U., Shutler, J. D., Valsala, V., Wanninkhof, R., and Zeng, J.: Data-based estimates of the ocean carbon sink variability – first results of the Surface Ocean $p\text{CO}_2$ Mapping intercomparison (SOCOM), *Biogeosciences*, 12, 7251–7278, <https://doi.org/10.5194/bg-12-7251-2015>, 2015.
- Rodgers, K. B., Aumont, O., Mikaloff Fletcher, S. E., Plancherel, Y., Bopp, L., de Boyer Montégut, C., Iudicone, D., Keeling, R. F., Madec, G., and Wanninkhof, R.: Strong sensitivity of Southern Ocean carbon uptake and nutrient cycling to wind stirring, *Biogeosciences*, 11, 4077–4098, <https://doi.org/10.5194/bg-11-4077-2014>, 2014.
- Rosso, I., Mazloff, M. R., Verdy, A., and Talley, L. D.: Space and time variability of the Southern Ocean carbon budget, *J. Geophys. Res.-Ocean*, 122, 7407–7432, <https://doi.org/10.1002/2016JC012646>, 2017.
- Roy, T., Bopp, L., Gehlen, M., Schneider, B., Cadule, P., Frölicher, T. L., Segsneider, J., Tjiputra, J., Heinze, C., and Joos, F.: Regional impacts of climate change and atmospheric CO_2 on future ocean carbon uptake: A multi-model linear feedback analysis, *J. Climate*, 24, 2300–2318, <https://doi.org/10.1175/2010JCLI3787.1>, 2011.
- Sabine, C. L., Feely, R. A., Gruber, N., Key, R. M., Lee, K., Bullister, J. L., Wanninkhof, R., Wong, C. S., Wallace, D. W. R., Tilbrook, B., Millero, F. J., Peng, T. H., Kozyr, A., Ono, T., and Rios, A. F.: The oceanic sink for anthropogenic CO_2 , *Science*, 305, 367–371, <https://doi.org/10.1126/science.1097403>, 2004.
- Sallée, J. B., Wienders, N., Speer, K., and Morrow, R.: Formation of subantarctic mode water in the southeastern Indian Ocean, *Ocean Dyn.*, 56, 525–542, <https://doi.org/10.1007/s10236-005-0054-x>, 2006.
- Sallée, J. B., Shuckburgh, E., Bruneau, N., Meijers, A. J. S., Bracegirdle, T. J., Wang, Z., and Roy, T.: Assessment of Southern Ocean water mass circulation and characteristics in CMIP5 models: Historical bias and forcing response, *J. Geophys. Res.-Ocean*, 118, 1830–1844, <https://doi.org/10.1002/jgrc.20135>, 2013.
- Sarmiento, J. L. and Gruber, N.: Ocean Biogeochemical Dynamics, *Carbon N. Y.*, 67, <https://doi.org/10.1063/1.2754608>, 2006.
- Sarmiento, J. L., Gruber, N., Brzezinski, M. A., and Dunne, J. P.: High-latitude controls of thermocline nutrients and low latitude biological productivity, *Nature*, 427, 56–60, <https://doi.org/10.1038/nature02127>, 2004.
- Sarmiento, J. L., Hughes, T. M. C., Stouffer, R. J., and Manabe, S.: Simulated response of the ocean carbon cycle to anthropogenic climate warming, *Nature*, 393, 245–249, <https://doi.org/10.1038/30455>, 1998.
- Séférian, R., Bopp, L., Gehlen, M., Orr, J. C., Ethé, C., Cadule, P., Aumont, O., Salas y Méliá, D., Voltaire, A., and Madec, G.: Skill assessment of three earth system models with common marine biogeochemistry, *Clim. Dynam.*, 40, 2549–2573, <https://doi.org/10.1007/s00382-012-1362-8>, 2013.
- Segsneider, J. and Bendtsen, J.: Temperature-dependent remineralization in a warming ocean increases surface $p\text{CO}_2$ through changes in marine ecosystem composition, *Glob. Biogeochem. Cy.*, 27, 1214–1225, <https://doi.org/10.1002/2013GB004684>, 2013.
- Son, S. W., Gerber, E. P., Perlwitz, J., Polvani, L. M., Gillett, N. P., Seo, K. H., Eyring, V., Shepherd, T. G., Waugh, D., Akiyoshi, H., Austin, J., Baumgaertner, A., Bekki, S., Braesicke, P., Brühl, C., Butchart, N., Chipperfield, M. P., Cugnet, D., Dameris, M., Dhomse, S., Frith, S., Garny, H., Garcia, R., Hardiman, S. C., Jöckel, P., Lamarque, J. F., Mancini, E., Marchand, M., Michou, M., Nakamura, T., Morgenstern, O., Pitari, G., Plummer, D. A., Pyle, J., Rozanov, E., Scinocca, J. F., Shibata, K., Smale, D., Teyssdre, H., Tian, W., and Yamashita, Y.: Impact of stratospheric ozone on Southern Hemisphere circulation change: A multimodel assessment, *J. Geophys. Res.-Atmos.*, 115, 1–18, <https://doi.org/10.1029/2010JD014271>, 2010.
- Swart, N. C., Fyfe, J. C., Saenko, O. A., and Eby, M.: Wind-driven changes in the ocean carbon sink, *Biogeosciences*, 11, 6107–6117, <https://doi.org/10.5194/bg-11-6107-2014>, 2014.
- Tagliabue, A., Mtshali, T., Aumont, O., Bowie, A. R., Klunder, M. B., Roychoudhury, A. N., and Swart, S.: A global compilation of dissolved iron measurements: focus on distributions and processes in the Southern Ocean, *Biogeosciences*, 9, 2333–2349, <https://doi.org/10.5194/bg-9-2333-2012>, 2012.
- Tagliabue, A., Williams, R. G., Rogan, N., Achterberg, E. P., and Boyd, P. W.: A ventilation-based framework to explain the regeneration-scavenging balance of iron in the ocean, *Geophys. Res. Lett.*, 41, 7227–7236, <https://doi.org/10.1002/2014GL061066>, 2014.
- Takahashi, T., Olafsson, J., Goddard, J. G., Chipman, D. W., and Sutherland, S. C.: Seasonal variation of CO_2 and nutrients in the high-latitude surface oceans: A comparative study, *Glob. Biogeochem. Cy.*, 7, 843–878, <https://doi.org/10.1029/93GB02263>, 1993.
- Takahashi, T., Sutherland, S. C., Sweeney, C., Poisson, A., Metzl, N., Tilbrook, B., Bates, N., Wanninkhof, R., Feely, R. A., Sabine, C., Olafsson, J., and Nojiri, Y.: Global sea-air CO_2 flux based on climatological surface ocean $p\text{CO}_2$, and seasonal biological and temperature effects, *Deep. Res. Pt. II*, 49, 1601–1622, [https://doi.org/10.1016/S0967-0645\(02\)00003-6](https://doi.org/10.1016/S0967-0645(02)00003-6), 2002.
- Takahashi, T., Sutherland, S. C., Wanninkhof, R., Sweeney, C., Feely, R. A., Chipman, D. W., Hales, B., Friederich, G., Chavez, F., Sabine, C., Watson, A., Bakker, D. C. E., Schuster, U., Metzl, N., Yoshikawa-Inoue, H., Ishii, M., Midorikawa, T., Nojiri, Y., Körtzinger, A., Steinhoff, T., Hoppema, M., Olafsson, J., Arnarson, T. S., Tilbrook, B., Johannessen, T., Olsen, A., Bellerby, R., Wong, C. S., Delille, B., Bates, N. R., and de Baar, H. J. W.: Climatological mean and decadal change in surface ocean $p\text{CO}_2$, and net sea-air CO_2 flux over the global oceans, *Deep. Res. Pt. II*, 56, 554–577, <https://doi.org/10.1016/j.dsr2.2008.12.009>, 2009.
- Takahashi, T., Sweeney, C., Hales, B., Chipman, D., Newberger, T., Goddard, J., Iannuzzi, R., and Sutherland, S.: The Changing Carbon Cycle in the Southern Ocean, *Oceanography*, 25, 26–37, <https://doi.org/10.5670/oceanog.2012.71>, 2012.
- Taylor, K. E., Stouffer, R. J., and Meehl, G. A.: An overview of CMIP5 and the experiment design, *B. Am. Meteorol. Soc.*, 93, 485–498, <https://doi.org/10.1175/BAMS-D-11-00094.1>, 2012.
- Thomalla, S. J., Fauchereau, N., Swart, S., and Monteiro, P. M. S.: Regional scale characteristics of the seasonal cycle of chlorophyll in the Southern Ocean, *Biogeosciences*, 8, 2849–2866, <https://doi.org/10.5194/bg-8-2849-2011>, 2011.
- Thompson, D. W. J., Solomon, S., Kushner, P. J., England, M. H., Grise, K. M., and Karoly, D. J.: Signatures of the Antarctic ozone hole in Southern Hemisphere surface climate change, *Nat. Geosci.*, 4, 741–749, <https://doi.org/10.1038/ngeo1296>, 2011.

- Tjiputra, J. F., Roelandt, C., Bentsen, M., Lawrence, D. M., Lorentzen, T., Schwinger, J., Seland, Ø., and Heinze, C.: Evaluation of the carbon cycle components in the Norwegian Earth System Model (NorESM), *Geosci. Model Dev.*, 6, 301–325, <https://doi.org/10.5194/gmd-6-301-2013>, 2013.
- Vichi, M., Pinardi, N., and Masina, S.: A generalized model of pelagic biogeochemistry for the global ocean ecosystem, Part I: Theory, *J. Mar. Syst.*, 64, 89–109, <https://doi.org/10.1016/j.jmarsys.2006.03.006>, 2007.
- Visinelli, L., Masina, S., Vichi, M., Storto, A., and Lovato, T.: Impacts of data assimilation on the global ocean carbonate system, *J. Mar. Syst.*, 158, 106–119, <https://doi.org/10.1016/j.jmarsys.2016.02.011>, 2016.
- Wanninkhof, R., Asher, W. E., Ho, D. T., Sweeney, C., and McGillis, W. R.: Advances in Quantifying Air-Sea Gas Exchange and Environmental Forcing, *Ann. Rev. Mar. Sci.*, 1, 213–244, <https://doi.org/10.1146/annurev.marine.010908.163742>, 2009.
- Wanninkhof, R., Park, G.-H., Takahashi, T., Sweeney, C., Feely, R., Nojiri, Y., Gruber, N., Doney, S. C., McKinley, G. A., Lenton, A., Le Quéré, C., Heinze, C., Schwinger, J., Graven, H., and Khatiwala, S.: Global ocean carbon uptake: magnitude, variability and trends, *Biogeosciences*, 10, 1983–2000, <https://doi.org/10.5194/bg-10-1983-2013>, 2013.
- Williams, N. L., Juraneck, L. W., Feely, R. A., Johnson, K. S., Sarmiento, J. L., Talley, L. D., Dickson, A. G., Gray, A. R., Wanninkhof, R., Russell, J. L., Riser, S. C., and Takeshita, Y.: Calculating surface ocean $p\text{CO}_2$ from biogeochemical Argo floats equipped with pH: An uncertainty analysis, *Glob. Biogeochem. Cy.* 31, 591–604, <https://doi.org/10.1002/2016GB005541>, 2017.
- Young, I. R.: Seasonal Variability of the Global Ocean Wind and Wave Climate, *Int. J. Clim.*, 19, 931–950, [https://doi.org/10.1002/\(SICI\)1097-0088\(199907\)19:9<931::AID-JOC412>3.0.CO;2-O](https://doi.org/10.1002/(SICI)1097-0088(199907)19:9<931::AID-JOC412>3.0.CO;2-O), 1999.
- Zahariev, K., Christian, J. R., and Denman, K. L.: Preindustrial, historical, and fertilization simulations using a global ocean carbon model with new parameterizations of iron limitation, calcification, and N_2 fixation, *Prog. Oceanogr.*, 77, 56–82, <https://doi.org/10.1016/j.pocean.2008.01.007>, 2008.
- Zickfeld, K., Fyfe, J. C., Eby, M., and Weaver, A. J.: Comment on “Saturation of the southern ocean CO_2 sink due to recent climate change”, *Science*, 319, 570, <https://doi.org/10.1126/science.1146886>, 2008.